

WATER TRANSPORT IN THE DIFFUSION MEDIA OF A PROTON EXCHANGE MEMBRANE FUEL CELL (PEMCF)

by

BYRON ALFONSO ZAMBRANO ROMAN

A thesis submitted in partial fulfillment of the requirements for the degree of

MASTER OF SCIENCE
in
MECHANICAL ENGINEERING

UNIVERSITY OF PUERTO RICO
MAYAGÜEZ CAMPUS
2009

Approved by:

Gustavo Gutierrez, PhD
Member, Graduate Committee

Date

Vikram Pandya, PhD
Member, Graduate Committee

Date

Stefano Leonardi, PhD
President, Graduate Committee

Date

Carlos Marin Martin, PhD
Representative of Graduate Studies

Date

Gustavo Gutierrez, PhD
Chairperson of the Department

Date

ABSTRACT

The fuel cell is an electrochemical energy conversion device that produces electricity based on an electrochemical reaction. From the diverse types of fuel cell the proton exchange membrane fuel cell (PEMFC) has better performance. Applications for this type of fuel cells are mostly in the transportation area where it serves as alternative power generation system [1]. Several researchers have found that the principal pivotal limitation in the performance in PEMFC is located at the cathode catalyst layer (CL) where oxygen reduction reaction takes place [11-14]. At high electric current density, water vapor, which is the product of this reaction, reach the condensation pressure and precipitate as liquid water reducing the active area of the CL. Gas Diffusion Layer (GDL) is inserted next to the catalyst layer in order to assist the CL with water drainage, trying to maintain the active area free of liquid. The present study will perform an 1-dimensional and 2-dimensional analysis of the water saturation in a GDL based in Darcy's law macroscopic approach, using the Unsaturated Flow Theory (UFT) and modeling the pressure in terms of water saturation with the experimental correlation called Leverett Function. Additionally, it will analyze in 1-dimension the effect of inserting Multiple Layers such as micro porous layers (MPL) and the influence of its morphological properties in the water transport.

This study also takes into account the effect of evaporation occurring close to the gas channel. The two phases are model as singles phases using the assumption that one movement mechanism at the time which was either as liquid water or vapor. It was found that the evaporation thickness increases at higher temperatures and decrease at higher gas channel relative humidity.

RESUMEN

Las celdas de combustible son dispositivos electroquímicos que producen energía eléctrica gracias a una reacción electroquímica. Existen una gran variedad de estos dispositivos siendo las celdas de combustibles de membrana de intercambio iónico (PEMFC) las que poseen un mayor desempeño. Aplicaciones para estos dispositivos se encuentran en su gran mayoría en el área de la transportación en donde sirve como un sistema alternativo de generación de electricidad [1]. Algunos investigadores han identificado que la mayor limitación para un mejor desempeño en este tipo de celdas se encuentra en la capa catalítica del cátodo, donde la reacción de reducción del oxígeno ocurre [11-14]. Una mayor limitante en la eficiencia se da a altas densidades de corriente, en donde; debido al flujo de generación de vapor, la presión del vapor de agua se incrementa igualando la presión de saturación, cambiando de estado de vapor a estado líquido. Esta agua en estado líquido cubre el área activa donde se realiza la reacción limitando el rendimiento de la celda de combustible. La membrana de difusión de gas (GDL) es insertada entre el canal de gas y la capa catalítica, con la función de proveer de oxígeno necesario para la reacción y para ayudar a drenar el agua, y así tratar de mantener el área activa libre de agua.

En el presente estudio se desarrolla un modelo numérico en donde se analiza la saturación de agua en una y dos dimensiones para una membrana de difusión de gas (GDL) basado en una aproximación macroscópica, usando la ley de Darcy y la teoría de flujo no saturado (UFT) y modelando la presión en términos de saturación de agua gracias a una correlación experimental llamadas funciones de Leverett.

También se analizó para una dimensión el efecto de insertar capas adicionales llamadas capas de poros microscópicos (MPL) y la influencia de sus propiedades morfológicas en el transporte de agua.

Este estudio toma en consideración el efecto de evaporación que ocurre cerca del canal de gas en el cátodo. Las dos fases son modeladas como una sola fase asumiendo un solo tipo de movimiento de fluido a la vez. Ya sea líquido o vapor. Se encontró que el frente de vaporización se incrementa a altas temperaturas y se disminuye y altos porcentajes de humedad relativa.

To my family . . .

ACKNOWLEDGEMENTS

To my advisor, Dr. Stefano Leonardi , for giving me the opportunity to learn from his knowledge and experience and to the research team for their support along this work.

Table of Contents

ABSTRACT.....	II
RESUMEN	III
ACKNOWLEDGEMENTS.....	VI
TABLE OF CONTENTS	VII
TABLE LIST.....	IX
FIGURE LIST	X
1 INTRODUCTION.....	2
1.1 OBJECTIVES	11
1.2 SUMMARY OF FOLLOWING CHAPTERS	12
2 THEORETICAL BACKGROUND	13
2.1 WATER TRANSPORT MECHANISM IN THE GAS DIFFUSION LAYER (GDL).....	13
2.1.1 Porosity (ϕ)	13
2.1.2 Permeability (k).....	13
2.1.3 Tortuosity.....	14
2.1.4 Wettability.....	14
2.1.5 Contact Angle (θ) and Surface Tension (σ).....	14
2.2 DARCY LAW	16
2.3 TWO PHASE FLOW IN POROUS MEDIA	17
2.3.1 Capillary Pressure.....	17
2.3.2 Saturation	20
2.3.3 Relative Permeability.....	20
2.4 CAPILLARY PRESSURE MODELS.....	22
2.4.1 Introduction to Capillary Pressure Models	22
2.4.2 Leverett Function.....	22
2.5 GAS PHASE TRANSPORT.....	23
2.5.1 General diffusion	23
2.5.2 Mass diffusivity.....	24
2.5.3 Gas-Phase in porous media.....	24
3 PREVIOUS WORK.....	26
4 ONE DIMENSIONAL ANALYSIS.....	30
4.1 ONE DIMENSIONAL WATER TRANSPORT ANALYSIS FOR SINGLE AND MULTILAYER DIFFUSION MEDIA	30
4.1.1 Model Assumptions.....	30
4.2 METHODOLOGY.....	31
4.2.1 Boundary Conditions	35

4.3	SINGLE LAYER RESULT	36
4.4	MULTILAYER DIFFUSION MEDIA	37
4.4.1	<i>Boundary conditions for Multilayer Diffusion Media</i>	37
4.5	MULTILAYER DIFFUSION MEDIA RESULTS	39
4.5.1	<i>Multilayer analysis Changing Morphological parameters</i>	40
5	TWO DIMENSIONAL WATER TRANSPORT ANALYSIS FOR SINGLE LAYER	
	DIFFUSION MEDIA.....	45
5.1	METHODOLOGY	45
5.2	COMPUTATIONAL DOMAIN AND BOUNDARY CONDITIONS.....	47
5.3	DISCRETIZATION	50
5.4	RESULTS	51
6	EVAPORATION THICKNESS	53
6.1	ASSUMPTIONS.....	53
6.2	METHODOLOGY	54
6.3	RESULTS	56
6.4	TWO DIMENSIONAL LIQUID FRONT.....	59
6.5	TWO DIMENSIONAL LIQUID FRONT METHODOLOGY	60
6.6	BOUNDARY CONDITIONS FOR TWO DIMENSIONAL MODEL	60
6.7	TWO DIMENSIONAL DIFFUSION EQUATION DISCRETIZATION.....	61
6.8	2-DIMENSIONAL RESULTS.....	63
7	CONCLUSIONS	67
APPENDIX A.	WATER SATURATION CODE.....	73

Table List

Tables	Page
TABLE 1.1 GDL Physics Properties	4
TABLE 4.1 GDL Physics Properties	35
TABLE 4.2 GDL, MPL Physics Properties	38
TABLE 4.3 GDL Physics Properties	49
TABLE 6.1 Evaporation Liquid front and diffusivity coefficient	57

Figure List

Figures	Page
Figure 1.1 Fuel Cell Cross Section [19].....	7
Figure 1.2 (a) SEM of Toray Paper GDL, (b) SEM of Carbon Cloth GDL [16]	9
Figure 2.1 Three Phase equilibrium surface tension γ_{sg} interfacial tension solid-gas, γ_{sl} interfacial tension solid-liquid, γ_{gl} interfacial tension gas-liquid, θ angle between γ_{gl} and γ_{sl}	15
Figure 2.2 (a) Hydrophobic Droplet contact angle measurement, (b) Hydrophilic Droplet contact angle measurement [16], (c) Microscopic view of a hydrophobic Droplet, (d) Microscopic view of a hydrophilic droplet [21].....	16
Figure 2.3 Measure of angle of contact in a single tube for a wetting and Nonwetting fluid, θ is the angle of contact [8].....	19
Figure 4.1 Schematic of water liquid saturation, water vapor and gas pressure profiles along GDL.....	31
Figure 4.2 Schematic GDL with its boundary conditions for 1 dimensional analysis....	36
Figure 4.3 Water Saturation Profile along Single Layer (GDM)	36
Figure 4.4 Schematics GDM for Multilayer indicating Multilayer Boundary condition	38
Figure 4.5 Water Saturation Profile along Multilayer GDM	39
Figure 4.6 Water Saturation Profile along DM Changing MPL Thickness	40
Figure 4.7 Water Saturation Average at different MPL Thickness.....	41
Figure 4.8 Water Saturation at the GDL-CL interface at different MPL Thickness....	42
Figure 4.9 Water Saturation along DM at different MPL Porosities	43
Figure 4.10 Water Saturation along DM at different MPL Contact Angle	44
Figure 5.1 Schematic for 2 dimension computational domain, where GDL refers to the gas diffusion layer and CCL refers to cathode catalyst layer	47
Figure 5.2 Boundary conditions for two dimensional model	49
Figure 5.3 two-dimensional water content color contour in a GDL at a current density of 2 A/cm ² under standard conditions	51
Figure 6.1 Scheme for 1-dimensional evaporation implementation.....	54
Figure 6.2 Evaporation thickness vs. temperature for different RH	58
Figure 6.3 Scheme of Liquid saturation and vapor concentration flux.....	59
Figure 6.4 Scheme of 2-dimensional domain boundary conditions.....	61
Figure 6.5 Scheme of two dimensional matching flux	62
Figure 6.6 2-dimensional contour water saturation implementing evaporation at different RH.....	64
Figure 6.7 2-dimensional contour vapor concentrations in terms of density at different RH.....	65

**Figure 6.8 2-dimensional water saturation and vapor concentration at different GDL
Temperatures. 66**

1 INTRODUCTION

A Fuel cell is an electrochemical conversion device that produces electricity based on an electrochemical reaction. This technology began at 1838 when a German chemist Christian Friedrich Schonbein conducted the first scientific research on a Fuel cell [1].

Other sources [2] affirm that Sir William Robert Grove, who introduced the concept of hydrogen Fuel cell, was the pioneer in this technology. However the decomposition of water into hydrogen and oxygen using electricity which is the inverse process occurring in a hydrogen fuel cell was not discovered until the earliest 1800 by British scientists Sir Anthony Carlisle and William Nicholson.

In the early 20th century, we have the first fuel cell with practical application manufactured by William W. Jecques. He was also the first to build high power systems fuel cells. During World War II; Thomas Francis Bacon developed a fuel cell to be use in submarines of the Royal Navy; the patent was latter acquired by Pratt & Whitney.

The Fuel cells developed since 1970 have been characterized by the following aspect: suppression of diffusion limitations in the electrodes to obtain a greater area of action, suppression of the costs of the catalysts, and increased performance and longer lifetime.

Nowadays fuel cells are widely used in the automobile industry and telecommunications industries. There are machines, traffic signals, laptops and portable electric devices powered by a fuel cell. Fuel cell for high scale applications can be seen as emergency power systems in Hospitals and Police station.

We can classify:

Stationary applications:

These applications are used to provide additional electrical power to power plants, or as independent power generation systems in isolated areas. This kind of applications today achieve an efficiency of 40% using hydrocarbon as a fuel and having an advantage of a quiet and not pollution generation system [18].

Applications for transport:

Applications for transport are the most promising applications for this alternative energy generation system. Over the last decade, automobile industries have been studying, developing and testing fuel cells to supply electricity to electric motors that in the future will replace the internal combustion engine. Some industries have already presented commercial models for example; at Los Angeles automobile saloon in 2007 Honda presented the model FCX Clarity. This is available since 2008 to the consumer.

In public transportation it also has been seen some advances concerning to this technology. In the last 4 years a large number of fuel cell buses operate worldwide. These vehicles are highly efficient as environmental friendly [1]. Table 1.1 shows a list of the fuel cell buses available and in use around the world.

TABLE 1.1 GDL Physics Properties

Manufacturer	Year	Fuel cell	Autonomy/Speed	
Volvo	2005	Ballard	563 km - 106 Km/h	
Mercedes Benz Citaro	2003	Ballard	200 km - 80 Km/h	
Bavaria	2000	Ballard	300 km - 80 Km/h	
Neoplan	2000	GmbH	250 km - 80 Km/h	
Van Hol	2006	UTC	400 km - 105 Km/h	
Toyota	2001	Toyota	300 km - 80 Km/h	

Fuel cell also becomes useful as auxiliary power units (APUS) in long-haul trucks. The Department of Energy of the United States (DOE) estimated about 1.17 billion dollars the annual cost of fuel for slow motion periods of truck (parking and rest periods for drivers). During this time, APU is supplying all electricity useful to the driver for heating, air conditioning, computer, TV, radio, refrigerator, microwave, etc.

Portable Applications:

Fuel cells are used to support as an auxiliary power system in military applications. Fuel cells are much lighter and more durable than batteries, which are particularly important for soldiers during periods of military maneuvers, end even more in case of war.

Micro Power:

Telecommunication companies as Motorola, Toshiba, Samsung, Panasonic, Sanyo and Sony have shown that mobile phones working with fuel cell can be run twice in comparison to those working with lithium battery with an equivalent size and it needs only 10 min to recharge with the necessary fuel.

Fuel cells can be classified referring to Temperature (high, medium, low), pressure of operation (high, medium, low) or according by the fuel and/or the oxidants they use (gaseous reactant, liquid fuel, solid fuels).

For practical reasons fuel cells are simply distinguish by the type of electrolyte used and the following names and abbreviations are now frequently used in publications: Alkaline fuel cells (AFC), phosphoric acid fuel cells (PAFC), molten carbonate fuel cells (MCFC), oxide fuel cells (SOFC) and polymer electrolyte fuel cells (PEMFC) [18].

Polymer Electrolyte Fuel Cell:

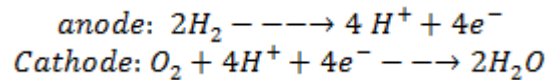
The present study will be focus in this type of cells motivated for its multiples advantage as high power density and that can vary their output quickly to meet shifts in power demand what makes this type perfect for automobile applications, where high performance and quick startup is required [1].

The electrolyte in this fuel cell is a Polymer membrane which is a good proton conductor but an electronic isolator.

PEMFC takes hydrogen as a Fuel that is consumed at the anode where oxidation of hydrogen take places, this reaction releases protons which are conducted through the Proton exchanges

membrane (PEM) to the cathode. Since PEM is an electrically insulator the electrons released for the hydrogen travel along the electrical detour provided and electrical current generated.

The Chemical reaction involved in this process is the following [20]



The only liquid in this fuel cell is water. The fuel cell must operate under conditions where the byproduct water does not evaporate faster than it is produced because the membrane must be hydrated. Because the limitation on the operating temperature imposed by the polymer and problems with water management the temperature of this type of cells must be less than 100 C.

The principal transport processes required for an operational fuel cell are:

1. Protons from the membrane to the cathode catalyst
2. Electrons from the current collector to the catalyst through the gas diffusion layer.
3. Transport of reactant (H_2) from the gas channel to the anode catalyst layer, and the same manner the transport of oxygen and water from and to the cathode catalyst layer to the cathode gas channel

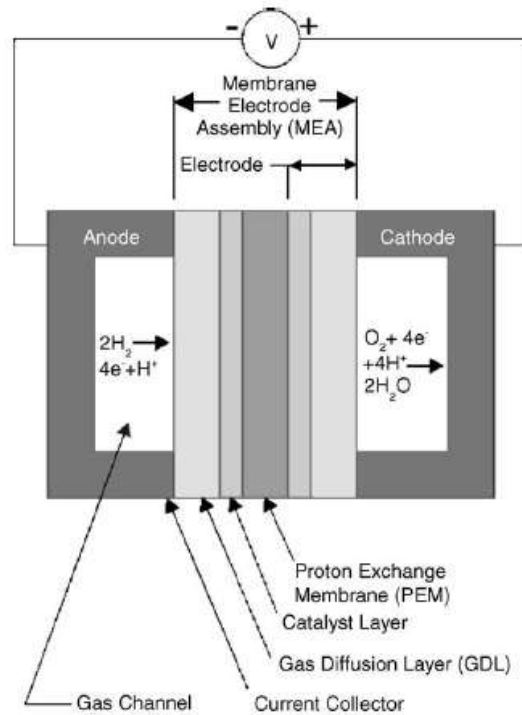


Figure 1.1 Fuel Cell Cross Section [19]

PEM fuel cells mainly consist of the anode and cathode gas channel which are the duct where oxygen and fuel gas streams are conducted. At the heart of the cells is the Membrane electrode assembly (MEA). The MEA is typically sandwiched by two flow field plates that are often mirrored to make a bipolar plate where cells are stacked in series for greater voltages.

The MEA is composed of a proton exchange membrane, catalyst layers, and Gas Diffusion layers at the anode and cathode side. Figure 1.1 shows the parts that compound a typical PEMFC.

Catalyst Layers

The catalyst layer is in direct contact with the membrane and the gas diffusion layer, it is also called the active layer. The objective is to place catalyst particles, platinum or platinum alloys within close proximity of the membrane.

This conventional catalyst layer generally features expensive platinum loading of 4 mg/cm^2 .

A large amount of research has been directed at reducing Pt loading as low as 0.014 mg/cm^2 [19].

There are a number of catalyst layer properties that have to be carefully optimized to achieve high efficiency of the catalyst material, and the level of hydrophobicity all have to be carefully balance.

Gas Diffusion layer

The porous gas diffusion layer in PEM fuel cells ensures that reactants effectively diffuse to the catalyst layer. In addition, the gas diffusion layer is the electrical conductor that transports electrons to and from the catalyst layer [23]. Typically, gas diffusion layers are constructed from a porous carbon paper or carbon cloth as figure 1.2 shows. This has a thickness in the range of 100-300 μm . The GDL also assists in water to reach, and be held at the membrane hydration. In addition, GDL are typically wet-proof with a PTFE (Teflon) coating to ensure that the pores of the gas diffusion layer do not become congested with liquid water.

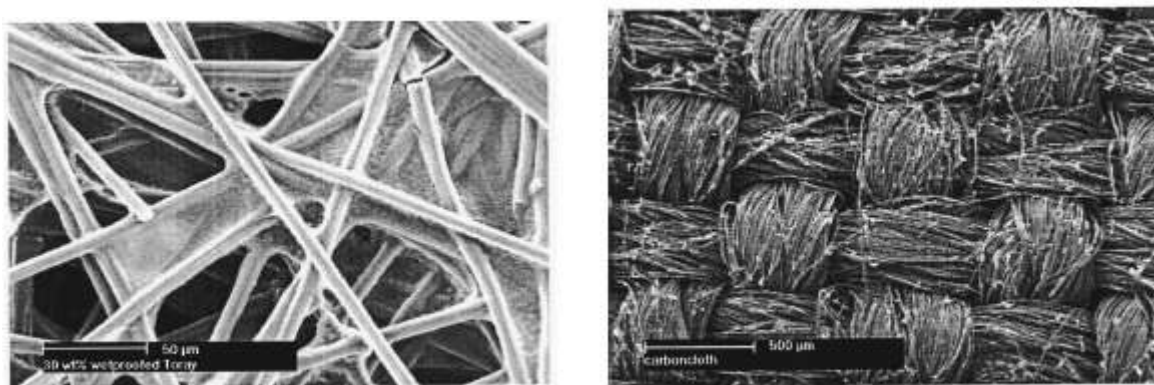


Figure 1.2 (a) SEM of Toray Paper GDL, (b) SEM of Carbon Cloth GDL [16]

The characteristic of the GDL as a porous medium have important influence on the cell performances. Important factors include properties as Permeability, porosity, wettability, thermal and electrical conductivity [17].

The species transport of gas and liquid is driven mostly by diffusion and capillary respectively and it is affected by porosity, whereas mass transport due to pressure difference is affected by permeability, cross-channel gas flow and liquid water flow from catalyst layer to gas channel.

In the last years the principal limitation in the performance of a PEM fuel cell has been the water management. At high current densities excessive production of water as a product of the reaction block reactant transport through GDL and incur mass transport losses. This phenomenon is known as “Flooding”. [10-17].

Flooding of the electrodes is generally associated to high-current density due to the higher water production rate, but it can occur at low-current densities under certain operation conditions like low temperatures or cold start when this fuel cell is applied to automobiles.

Several modeling studies have been published in order to predict the PEMFC performance at given flooding levels.

Water transport in PEMFCs is governed by the following phenomena [13]:

- Water generation at the cathode due to the oxygen reduction reaction (ORR)
- Forward and backward diffusion of water across the membrane
- Electro-osmotic drag of water
- Convective removal of water to the gas channel

The present analysis will focus in the water transport from the cathode catalyst layer using a macroscopic approach based on Darcy's law assuming unsaturated flow theory and modeling the pressure in terms of water saturation using the experimental correlation called Leverett Function.

1.1 Objectives

The aim of the present thesis is to study the water saturation in a Gas Diffusion Layer. The product of the oxygen reduction is water vapor; this water at high electric current densities exceeds the saturation pressure becoming liquid water. The excess of liquid water reduce the catalyst layer active area, this is called Flooding. The GDL is a porous media that helps to drainage the liquid water toward the gas channel. A numerical simulation will be performed based on a macroscopic Darcy`s law approach using Unsaturated Flow Theory modeling the pressure with an experimental correlation called Leverett function. The effect of water evaporation near the gas channel will be modeled assuming constant temperature. These results will be obtained through a code written in FORTRAN for one and two dimensions.

1.2 Summary of Following Chapters

The following two chapters will explain concepts as porosity, permeability, tortuosity and all the terminology used in this study. It will also explain Darcy's law which was used to model the water movement as the theoretical background used. It will also summarize previous work done experimentally as well as numerically by other researchers. Chapter 4 explains the approach made and presents the water saturation profile through the gas diffusion layer (GDL) and as additional work was analyzed the effect of multiple layers and the influence of its morphological characteristic discontinuities on the water saturation. Chapter 5 uses the same approach made by previous chapter performing a two dimensional approach. This two dimensional approach took in consideration the no flux land effect. The chapters 6 and 7 deal with the evaporation front for one and two dimensions. The evaporation front is the distance from the gas channel-GDL where the liquid phase completely disappears and the only way of water transport is through vapor diffusion. The last chapter summarized the most important conclusion based on the results found in this study.

2 THEORETICAL BACKGROUND

2.1 Water transport mechanism In the Gas Diffusion layer (GDL)

The Gas Diffusion Layers are porous structures that accomplish an important role in the fuel cell operation, providing the necessary oxygen to the reaction and draining the liquid water originated as a product of the reaction formed after the water reaches the condensation point. The porous media is characterized by the pore structure. The more important parameters are:

2.1.1 Porosity (ϕ)

Is the fraction of the bulk volume of the porous sample that is occupied by the pore or void space. Porous or void space can be divided in two types: one in which each pore is connected to other called “Interconnected” or “effective” pore spaces, and the other where the pore is not connected which is called “non-interconnected” pore or “void dispersed” [5].

2.1.2 Permeability (k)

Permeability is the ability of the porous structure in transport Newtonian Fluids. This property is of limited use because its dependence on the conductive fluid as porous sample properties. It is more scientific to measure the Permeability of the fluid independently of the fluid properties and flow mechanisms. This is called “specific permeability k ” or “Permeability”. [9].

2.1.3 Tortuosity

Tortuosity is a measure of the effective average path length through the porous media compared to the linear path length across the media in the direction of transport [8].

2.1.4 Wettability

The wettability is the affinity of the material with one or another fluid. This preferential water-wet is defined by Jennings (1958). When two or more fluids occupy a porous medium, one of the fluids is absorbed on the surface more strongly than the other fluid. The fluid absorbed is called wetting fluid and the fluid that is displaced is called non-wetting fluid. [8]

The wettability is also defined as the speed at which the fluid spread over solid surface. The speed of spreading is directly controlled by interfacial forces at the solid surface.

The spreading can be increased by lower surface tension and lower fluid viscosity. For two phases flow in porous media the wetting angle influences the capillary pressure and liquid transport considerably hence, it is an important parameter to be considered for water transport.

2.1.5 Contact Angle (θ) and Surface Tension (σ)

Contact angle is a critical parameter in two-phase flow defined as the angle between the gas-liquid interface and the solid surface [8].

This angle can be interpreted as a measure of the wettability of the solid surface by a liquid on different surfaces. Contact angle depend on the base material, surface temperature, surface impurities and surface roughness.

The contact angle can be obtained using a mechanical equilibrium relation derived by Young in 1800. The liquid droplet angle of any solid surface under the action of three interfacial tension (surface tension)[4]. The interfacial tension is defined as the amount of work that must be performed in order to separate a unit area of fluid from another.

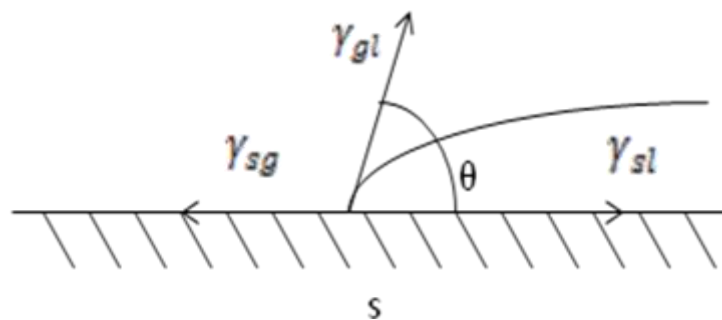


Figure 2.1 Three Phase equilibrium surface tension γ_{sg} interfacial tension solid-gas, γ_{sl} interfacial tension solid-liquid, γ_{gl} interfacial tension gas-liquid, θ angle between γ_{gl} and γ_{sl}

Figure 2.1 shows the interfacial tension from the solid-gas (σ_{sg}), solid-liquid (σ_{sl}) and gas-liquid (σ_{gl}) respectively. Using state equilibrium in the x direction we obtain the angle between the gas-liquid interfacial tension:

$$\cos \theta = \frac{\sigma_{sg} - \sigma_{sl}}{\sigma_{gl}} \quad 2.1$$

Depending upon the molecular force balance at the contact line, the surface tends to extent or contract. The relation between the wettability nature of the porous material and the contact angle is as follow:

$\theta < 90$ the fluid is termed wetting and the surface is Hydrophilic to the fluid.

$\theta > 90$ the fluid is termed non-wetting and the surface is Hydrophobic to the fluid.

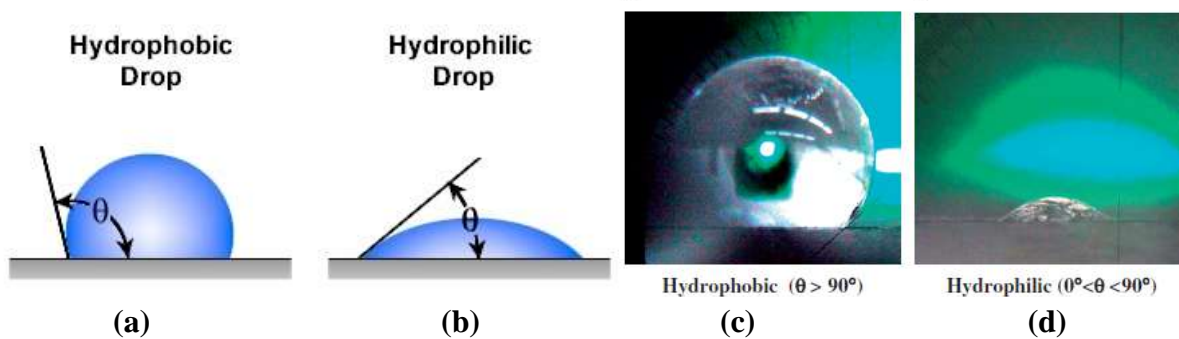


Figure 2.2 (a) Hydrophobic Droplet contact angle measurement, (b) Hydrophilic Droplet contact angle measurement [16], (c) Microscopic view of a hydrophobic Droplet, (d) Microscopic view of a hydrophilic droplet [21]

2.2 Darcy Law

Darcy, with his experiment defined the permeability K in terms of a new unit called Darcy. This is part of the definition of his law; which is a linear law and it is analogue to the Newton`s law of viscosity, Ohm`s law of electricity, Fourier`s law of heat conduction and Fick`s law of diffusion [5].

Darcy formulated this law based in his experiment where he measured the volume flow rate Q, through a cylinder of circular cross section A and a length L, hydrostatic pressure drop $\Delta P = P_1 - P_2$. The following relation was found:

$$Q = \frac{KA}{\mu_l} \frac{(P1 - P2)}{L} \quad 2.2$$

Where μ is the viscosity of the fluid. This experiment measured the permeability of a porous media and introduced the Darcy unit which is define as the amount of substance that flow with a flow rate of 1 cm³/s with a viscosity of 1cp (cp=centipoises=10E-3 Pa-s) though a cube having sides of 1 cm in length, if the pressure difference is 1 atm[9].

$$1 \text{ darcy} = \frac{1 \left(\frac{\text{cm}^3}{\text{s}} \right) 1(\text{cp})}{1(\text{cm}^3) 1 \left(\frac{\text{atm}}{\text{cm}} \right)} \quad 2.3$$

2.3 Two Phase flow in porous media

The GDL is the essential component of PEMFC. It is a porous media which provide the necessary reactant to the catalyst and remove water at the cathode which is the product of the reaction. This product primarily moved by capillarity forces.

2.3.1 Capillary Pressure

Since two or more fluid coexist in a system, there exist a pressure difference at the interface between the phases due to the interfacial tension caused by the imbalance of the molecular forces at the line of contact. This pressure difference between these two phases is defined as capillary pressure. Suppose air as a wetting fluid filling all the space in the GDL. Assuming

atmospheric pressure for the wetting phase (air), the non-wetting fluid will not spontaneously penetrate and displace the wetting phase unless that the non-wetting fluid pressure exceed the wetting phase pressure. Then the capillarity pressure is defined as the difference between the wetting and the non-wetting phase [6][4].

$$P_c = P_w - P_{nw} = \sigma \left(\frac{1}{r'} + \frac{1}{r''} \right) \quad 2.4$$

Here r' and r'' are the two principal radii between the liquid and the solid pore surface.

Equation 2.4 is also known as Laplace equation for capillary pressure. Most modeling studies of fuel cells assume a capillary tube model, in which the porous media is composed of tubes of different size where R is the mean value of the radii [9]. The capillary pressure for the tube can be rewritten as:

$$P_c = \frac{2\sigma_{gl} \cos \theta}{R} \quad 2.5$$

Where σ is the surface tension, R the Radii of the wetting phase and θ is the angle between two fluids interface and the solid phase. We can understand the basic principles involved in capillary flow by considering a single capillary column, as figure 2.3 shows.

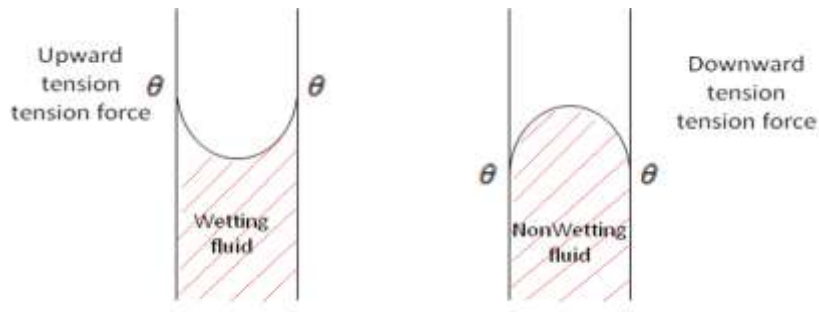


Figure 2.3 Measure of angle of contact in a single tube for a wetting and Nonwetting fluid, θ is the angle of contact [8]

If the capillary tube is hydrophilic to the fluid, a net capillary suction force will draw fluid up the walls of the tube until the gravity force balances the surface tension force. If the capillary tube is hydrophobic to the fluid, the meniscus will concave down as the figure 2.3 depicts; thus we have the following relation depending on the wettability nature of the porous medium [13].

$$P_c = P_w - P_{nw} \quad 2.4$$

$$P_c < 0 \Leftrightarrow P_w > P_{nw} \quad \text{for } \theta < 90^\circ \quad \text{Hydrophilic}$$

$$P_c > 0 \Leftrightarrow P_w < P_{nw} \quad \text{for } \theta > 90^\circ \quad \text{Hydrophilic}$$

The resulting pressure difference can cause water to flow from high capillary pressure areas to low capillary pressure areas.

In fuel cell studies, it is reasonable to assume immiscible flow meaning we treat the gas phase and the liquid phase as non-mixing; this allows separating the phases into wetting and non-wetting components.

In fuel cell application the increase of the capillary pressure is associated to the water generation due to the oxygen reduction reaction in the Catalyst layer. At lower current

density on standard fuel cell conditions the product of the reaction at the cathode catalyst layer is water vapor, but at certain conditions as lower temperatures or at high current densities the vapor pressure increase reaching the water saturation pressure becoming liquid. This liquid water penetrates the porous media thus reducing the performance of the fuel cell. [11-17].

2.3.2 Saturation

In two-phase systems, the volume fraction of total pore volume occupied by a phase is termed the phase saturation. Saturation S , is a key parameter for multiphase flow, because it represents the available volume through which both phases can still flow. The phase saturation (S_i), is expressed as:

$$S_i = \frac{\text{Volume of fluid Phase}}{\text{Total accesible pore volume}} \quad 2.6$$

For liquid water saturation in a hydrophobic medium it is measured assuming that wetting phase (air) is fully saturated and the liquid water is infecting very slowly increasing capillary pressure applied to it.

2.3.3 Relative Permeability

In Two-phase flow in porous media, the available pore space is shared by the two phases. We could define the relative permeability as the ratio of the actual permeability for a phase at a given saturation to the total intrinsic permeability of the porous media:

$$K_r = \frac{K}{K_{\text{abs}}} \quad 2.7$$

Mathematical approach based on previous experiments are commonly preferred for estimating the relative permeability because of the difficulty in conducting direct experiments. Most of the relative permeability correlations are bases in physical models. Typically, the general shape of the relative permeability curves can be estimated by following equations [11][8]:

$$K_{r,nw} = A(S_{nw})^n \quad \text{and} \quad K_{r,nw} = B(1 - S_{nw})^m \quad 2.8$$

Where nw and w represent wetting and non-wetting fluids, respectively and A and B, n and m are constant depending upon the structure of the porous media.

In fuel cell applications, a typical relative permeability expression [$K_r = s_{nw}^3$] for nonconsolidated sands is adapted to describe the phase transport in Diffusion media due to its simplicity.

2.4 Capillary Pressure Models

2.4.1 Introduction to Capillary Pressure Models

Several researchers have been tried to model the capillary pressure since a direct measure of the contact angle (θ) and the radii of each pore is very difficult.

Several empirical and semi empirical expression which attempt to describe the behavior of capillary pressure in terms of a porous media and fluid properties are available in literature. Capillary pressure depends on a variety of parameters, including temperature through surface tension and morphology, tortuosity, and pore size of the material but most importantly liquid saturation. A generic Leverett function is often used to describe the capillary transport behavior of the porous media in multiphase models.

2.4.2 Leverett Function

Leverett (1941) defined a dimensionless capillarity pressure function, which was subsequently named the Leveret J function by Rose and Bruce (1949). Characteristic of different type of porous media Leverett type function has been used to represent the behavior as a first step forward achieving an accurate two-phase transport model.

The dimensionless Leverett function is described as follow[24]:

$$J(S_w) = \frac{P_c}{\sigma \cos \theta} \sqrt{\frac{K}{\phi}} = f(S_w) \dots (1) \quad 2.9$$

The Leverett function is function of Surface tension (σ), Capillarity pressure (P_c) and porous properties as permeability (k) and porosity (ϕ). The Leverett approach incorporates the effect of interfacial tension but uses a simple relation $[k/\phi]^{0.5}$ for the average pore radius basically ignoring the tortuous nature of the porous media. But $J(s)$ function represents the Leverett function for scaling drainage capillary pressure curves obtained experimentally and it is described as follow [8][17][11].

$$J(s_l) = \begin{cases} 1.417(1-s_l) - 2.120(1-s_l)^2 + 1.263(1-s_l)^3 & \text{if } \theta < 90^\circ \longrightarrow \text{Hydrophilic} \\ 1.417s_l - 2.120s_l^2 + 1.263s_l^3 & \text{if } \theta > 90^\circ \longrightarrow \text{Hydrophobic} \end{cases}$$

2.10

Although this approach serves as a useful starting point, the applicability of a generic Leverett function to the highly anisotropic thin-film diffusion media is unclear and unverified. Specific concerns are based on the differences in the Fuel cell diffusion media and conditions under which the Leverett function was derived (sand).

2.5 Gas Phase Transport

2.5.1 General diffusion

Diffusion is the net transport of molecules from a region of higher concentration to one of lower concentration by random molecular motion [7][25]. This motion tends to reach the steady state condition by mixing the molecules and eliminating the concentration gradient of a specific fluid.

The equation that governs this motion is known as Fick's law, and is analogue to heat transfer equation (Fourier's law).

A binary mixture of A and B species, it may be express in vector form as:

$$J_A = -\rho D_{AB} \nabla m_A \quad 2.11$$

2.5.2 Mass diffusivity

The diffusivity coefficient assuming ideal gas behavior, kinetic theory may be used to show that.

$$D_{AB} \sim P^{-1} T^{3/2} \quad 2.12$$

Where T is expressed in Kelvin, this relation applies for restricted pressure and temperature ranges and it is useful for estimating values of the mass diffusivity at conditions other than those for which data are available.

2.5.3 Gas-Phase in porous media

The inhibition must be related to two factors:

Porosity: at zero porosity, the effective gas-phase diffusivity must be zero. At porosity of 1, the effective diffusivity must be equal to bulk value.

Tortuosity: the more tortuous the path, the longer the effective path length through the media, and the greater reduction the effective diffusivity [8]. The effective diffusivity for gas-phase flow in porous media can be written as:

$$D_{eff} = D \frac{\phi}{\tau} \quad 2.13$$

Where D_{eff} is the effective bulk gas-phase diffusivity in the porous media ϵ is the porosity, D is the diffusivity in gas, and τ is the Tortuosity. Since Tortuosity is a difficult parameter to

estimate except through direct experiment, a Bruggeman correlation is often used for fuel cell studies. This relationship assumes τ is proportional to $\phi^{-0.5}$ resulting in the simpler expression:

$$D_{eff} = D\phi^{1.5} \quad 2.14$$

The Binary Gas-Phase diffusion coefficient can be estimated with many different approaches. Based solely on molecular Dynamic theory, we can derive:

$$D_j = \frac{T^{3/2}}{P \cdot MW^{1/2} \sigma^2} \quad 2.15$$

This is a simple expression of self-diffusion of species j into a mixture of j. Independent of other species, where σ is the collision diameter of the molecule, P the pressure of the mixture j and MW the molecular weight.

Another way to quickly obtain approximate data is to assume the functional dependence of pressure and temperature in equation 2.15 [21] [8] and extrapolate from known experimental data taken from Y. Wang and C. Y. Wang [22]. That is,

$$D_{12}(T, P) = D_{12, Known}(T_{ref}, P_{ref}) \left(\frac{T}{T_{ref}} \right)^{3/2} \left(\frac{P_{ref}}{P} \right) \quad 2.16$$

This will provide fairly accurate results as well, especially for non polar molecular. In summary, there are several approaches of varying complexity and precision available to estimate the gas-phase diffusivity. The choice taken depends on the level of precision required. Direct experimental data for all modes of transport are always preferred over generalized correlation.

3 PREVIOUS WORK

The prediction of water movement or water content into a porous structure is still not completely understood and a motivation for researches. Several authors have developed macroscopic models as experimental prediction.

In the experimental field Gostick et al[10] calculated and expressed the capillary pressure in terms of saturation of the wetting phase for several GDL that are commonly used in the fuel cell. Gostick used two techniques; the Mercury intrusion porosimetry (MIP) and the Method of Standard porosimetry (MSP). This technique could also measure the capillary in all the pores and in the hydrophilic ones. It was found that the hydrophilic pores have the same shape as the overall Porous media. The experimental data obtained was correlated with the Leveret J-Function.

F.T. Zhang et al [14], studied experimental and theoretically liquid water transport for the Gas diffusion layer and gas channel using a transparent Proton exchange fuel cell. They also studied the effect of cathode air flow rate on the liquid water distribution and cell performance. In the images published in this paper it can be appreciated that the water appears in the form of droplets due to the GDL hydrophobic nature. For low air velocities, the mechanism of liquid water removal from the GDL surface is by droplet detachment through the shear force exerted by the gas core flow at high air velocities and by capillary wicking onto hydrophilic channel walls at low air velocities.

Kumbur et al [11] developed one dimensional steady state theoretical model with a relation pressure-saturation based on the experimental data reported by Gostick. This study also obtained a new permeability correlation by fitting the experimental capillary pressure data into four well established empirical models. The models predicted the saturation isolated all the effects as humidity, two dimensional effects, inlet conditions and time dependence parameters. The found a new relation that has better accuracy under limited conditions.

He et al [12] developed two phase flow, steady state two-dimensional model to study the effects of the gas and liquid transport with the increase of the oxygen flow rate. This article also studied the effect of the Electrode thickness that is associated with the Gas Diffusion layer thickness due to the fix fuel cell thickness. The Authors used the Darcy model to describe the transport of the gas phase. Transport of liquid water through the porous electrodes is driven by the shear force of gas flow and capillary forces. Depending in the local partial pressure of water and its saturation vapor pressure at the operation temperature, water can evaporate or condense. The effect of condensed and evaporated water is taken in to account for this model.

They found that higher pressure drop yields higher electrodes performance because the oxygen transport rate is higher and liquid water transport is more effective. The author recommends a electrode thickness optimization to get an optimal performance.

Z.H. Wanga et al [15] developed a numerical model, two-phase, steady state capable to simulate the process at single-phase, which occurs at low current densities and the process

where a single-phase region co-exists with a two-phase zone in the air cathode. The authors also defined an expression in order to obtain the threshold current density corresponding to the first appearance of liquid water at the membrane/cathode interface. This model is also capable to predict the transition between these two regimes.

Liquid and vapor water movements are controlled by capillary action and molecular diffusion respectively.

Passaogullari and Wang [13] developed a one-dimensional, steady state theoretical model from a cross section of the entire Fuel cell. This author used Darcy law and modeled capillary pressure with the standard Leverett function. The relative permeability is modeled in terms of water saturation, it is assumed a fully saturated water vapor and that the only mode of water transport is in liquid state, it is introduced the effect of reduction of the active area by the water liquid saturation. They estimated the onset of the two phase regime in GDL's and the associated threshold current density as a function of various anode and cathode relative humidity combinations.

They also derived an analytical solution of one dimensional model for liquid water transport in both hydrophobic and hydrophilic porous media in order to study the influence of the wettability of the Gas diffusion layer in the water transport. Finally this article predicts a significant decrease in performance with the increase of the saturation level, in particular at high current density in accordance with experimental observations.

Passaogullari and Wang et al [17] created a one dimensional model in order to predict the liquid water saturation along the Cathode Gas diffusion layer (GDL) assuming M2 model approach and Leverett function approach. These approaches were solved numerically by

using a Runge-Kutta method with adaptive step size with a local current density of 2 A/cm². It was found that M2 model predict higher saturation profile than Leverett UFT model approach, that occurs because M2 model take in to account the small variation of gas pressure that Leverett UTF method assumed constant.

Using the M2 model created by the authors it was analyzed the effect of multilayer diffusion media and the interface in the liquid water transport. Finally they studied the effect of porosity, thickness and wettability of a micro-porous layer (MPL) on the two-phase transport in the Proton exchange membrane fuel cell.

Based on Passaogullari and Wang [17] work the present study will analyze as first step the liquid water transport along the cathode gas diffusion layer in one dimensional analysis using the Leverett function approach and then analyze the effect of a multilayer with this type of approach. As an intermediate step we have studied the effect of changing the material morphological properties in the liquid water transport. After having studied these effect we have developed a two dimensional model of these approaches.

4 ONE DIMENSIONAL ANALYSIS

4.1 One Dimensional water transport analysis for single and multilayer Diffusion media

One dimensional analysis has the goal to determine the water saturation profile along the Cathode Gas Diffusion Layer (GDL). This step serves as insight to asses one of the main goal of this study. This analysis is performed numerically using a fourth order Runge-Kutta method maintaining the same step size in contrast from the study done by Pasaogullari and Wang [17]. The results of this approach will be validated with [17], and in addition it will be analyzed the effect of the multilayer morphological properties on the water transport in a multilayer diffusion media. This analysis will be performed with a standard Leverett function with an Unsaturated Flow Theory approach in comparison with the M^2 method of Pasaogullari and Wang [17] and takes the effect of air pressure and sink and source terms as its principal characteristic.

4.1.1 Model Assumptions

The assumptions made for the present model are the followings:

- Steady State conditions
- Isothermal
 - GDL maintains the same temperature along all the domain
- Two Phase flow is modeled with unsaturated flow theory (UFT)
 - This implies that Gas Phase pressure is constant across the porous medium.
- Liquid phase flux is expressed by Darcy`s Law

- No net gas phase diffusion
 - Water vapor is saturated along the gas Diffusion layer.
- The Only mode of water transport is capillary transport of liquid water.
 - All the water produced at the catalyst layer is conducted through the Gas Diffusion Layer in Liquid state.
- Reduction reaction occurs at the GDL-Catalyst layer interface
 - This is justified by the dimension of the catalyst layer which is very small in comparison to the Diffusion media.

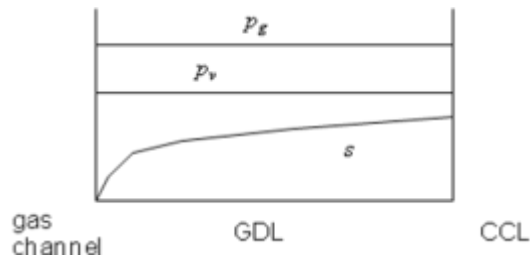


Figure 4.1 Schematic of water liquid saturation, water vapor and gas pressure profiles along GDL

4.2 Methodology

The governing equations for liquid-water transport are obtained from in the continuity equation, which is:

$$\frac{\partial(\phi_l s)}{\partial t} + \nabla(\rho_l u) = 0 \quad 4.1$$

The net flux across the membrane from anode to cathode is assumed to be constant and characterized by a net water transport coefficient α . By combining the net water transport with water production integrated over the GDL, under steady state conditions we have:

$$\nabla(\rho_l u) = -\frac{I}{2F}(2\alpha + 1)M^{H_2O} \quad 4.2$$

Where F is the faraday constant which is a measure of the electric charge per unit electrons and it has a value of 96485.33 C/mol. “I” represent the current electric density, for this analysis it was used a current density of 2 A/cm² because it is known that at chosen current density under standard conditions must occur GDL flooding, and M^{H_2O} represent the molar mass of water.

The left-hand sides of the continuity equation (Eq.4.2) represent the liquid water inlet which is the water generated by the catalyst layer product of the oxygen reduction reaction plus the net water transport.

Liquid water flux is expressed by Darcy's Law as:

$$u_l = -\frac{Kk_{rl}}{\mu_l} \nabla P_l \quad 4.3$$

Where the liquid water pressure is obtained from the capillary pressure which is defined as the difference between the air pressure (P_g) and the water pressure (P_l)

$$P_c = P_l - P_g \quad 4.4$$

Unsaturated Flow Theory (UFT) state that the gas Phase pressure is constant across the entire porous layer by the following expression

$$P_l = P_c + P_g \quad \nabla P_c = \nabla P_l \quad 4.5$$

Combining Equation (4.5) with Equation (4.3) we have:

$$u_l = -\frac{Kk_{rl}}{\mu_l} \nabla P_c \quad 4.6$$

Where k_{rl} is the relative permeability of the liquid phase and it is modeled in terms of water saturation as:

$$k_{rl} = S^3 \quad 4.7$$

The capillary pressure between the gas and liquid phases can be related to the phase saturation via

$$P_{cl} = \sigma \cos \theta_c \left(\frac{\phi}{K} \right)^{1/2} J(s) \quad 4.8$$

This relationship is obtained from the definition of the Leverett function where the radii are expressed in terms of porosity and intrinsic permeability. Leverett function is modeled using the following correlation:

$$J(s_l) = \begin{cases} 1.417(1-s_l) - 2.120(1-s_l)^2 + 1.263(1-s_l)^3 & \text{if } \theta < 90^\circ \longrightarrow \text{Hydrophilic} \\ 1.417s_l - 2.120s_l^2 + 1.263s_l^3 & \text{if } \theta > 90^\circ \longrightarrow \text{Hydrophobic} \end{cases} \quad 4.9$$

As we mentioned in the previous chapter the Leverett function is expressed as function of the wetting phase therefore in hydrophilic GDL ($\theta < 90$) Leverett function were in terms of air saturation, then we had changed it as a function of liquid saturation.

Combining the Darcy's law (Eq.4.6) with the Unsaturated Flow Theory, liquid water flux is expressed in terms of liquid saturation.

$$u_l = -\frac{Kk_{rl}}{\mu_l} \sigma \cos \theta_c \left(\frac{\phi}{K} \right)^{1/2} J(s) \quad 4.10$$

Combining the water flux with Equation (4.2) we obtain the follow relation:

$$-\frac{Kk_{rl}}{v_l} \sigma \cos \theta_c \left(\frac{\phi}{K} \right)^{1/2} J(s) = -\frac{I}{2F} (2\alpha + 1) M^{H_2O} \quad 4.11$$

This equation expresses the water transport usually known as Richards Equation and it is solved similar to a diffusion equation, where D_c is:

$$D_c = \frac{\sigma \cos \theta}{v_l} (\phi K)^{1/2} (s^3) \frac{dJ(s)}{ds} \quad 4.12$$

Rearranging Equation 4.11 we have:

$$-D_c \nabla s = -\frac{I}{2F} (2\alpha + 1) M^{H_2O} \quad 4.13$$

As it was mentioned above this equation reduced to a First Order Ordinary differential equation and it was solved numerically by a fourth order Runge-Kutta numerical method in order to achieve this previous step. This subroutine was written in FORTRAN.

4.2.1 Boundary Conditions

Because equation 4.13 is an ordinary differential equation it needs a boundary condition which is at the Gas channel-GDL interface. Here we assumed no water saturation. The boundary conditions and computational domain are represented in figure 4.2

The dimensional properties of the GDL are described in Table 4.1:

TABLE 4.1 GDL Physics Properties

Physics Properties		Unit	Value
Total Cathode gas Diffuser Thickness		μm	300
GDL Contact Angle	θ	$^{\circ}$	108
GDL Porosity	ϵ_{GDL}		0.4
GDL Permeability	K_{GDL}	m^2	5.00e-13
Surface tension liquid-water-air (80°C)	σ	(N/m)	0.0625
Liquid water viscosity (80°C)	μ_1	(Pa.s)	30
Liquid water density (80°C)	ρ	(Kg/m ³)	5
cell temperature	T_{cell}	$^{\circ}\text{C}$	11
Net water transport coefficient	α		0.5

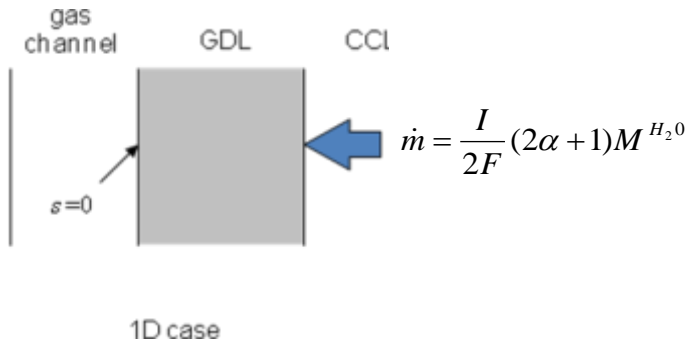


Figure 4.2 Schematic GDL with its boundary conditions for 1 dimensional analysis

4.3 Single Layer Result

This approach is valid for either carbon cloth or carbon paper. At GDL-Gas channel interface the saturation gradient is higher than on the other boundary therefore an appropriate step size is necessary in order to obtain accurate results.

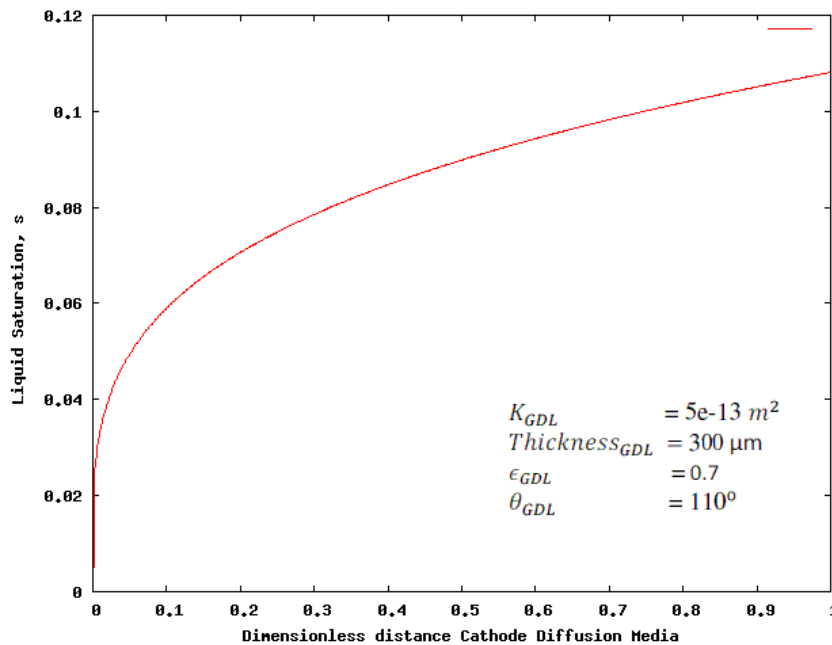


Figure 4.3 Water Saturation Profile along Single Layer (GDM)

The figure 4.3 is the predicted water saturation profile obtained. It can be noticed that on the left side, where the gas channel-GDL interface is located, the liquid saturation gradient is higher and start to decrease as it gets closer to the catalyst layer interface. These results agree well with Pasaogullari and Wang [17].

4.4 Multilayer Diffusion Media

Some authors [13][11] have predicted that with the introduction of different layers with higher permeability one could increase the liquid water drainage; these layers are known as Micro Porous Layer (MPL).

Micro porous layer increases the Liquid pressure therefore increasing the capillary pressure that is the principal mechanism for liquid water movement from the CL to the MPL-GDL interface. The different morphological characteristic between GDL and MPL caused a discontinuity in liquid water saturation at the interface between these two layers. The magnitude of the discontinuity does not depend only on the material properties of these two layers but it also depends in the liquid water flux. In order to solve the water saturation profile we need to find a relation to predict this water drop or water saturation discontinuity.

4.4.1 Boundary conditions for Multilayer Diffusion Media

The boundary condition for the GDL-MPL interface is obtained from the capillary pressure condition which is know that is continuous through the interface between these two layers.

$$P_c^{GDL} = P_c^{MPL} \quad 4.14$$

Therefore:

$$\cos \theta_c^{GDL} \left(\frac{\phi^{GDL}}{K^{GDL}} \right)^{1/2} J(s^{GDL}) = \cos \theta_c^{MPL} \left(\frac{\phi^{MPL}}{K^{MPL}} \right)^{1/2} J(s^{MPL}) \quad 4.15$$

This is the governing relationship in the interface. Based in this relation it is obtained the boundary condition needed for the MPL in order to apply the same numerical method.

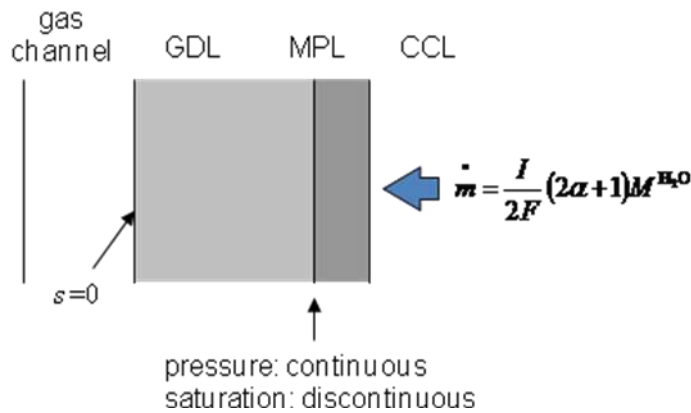


Figure 4.4 Schematics GDM for Multilayer indicating Multilayer Boundary condition

The physical properties of the MPL are described in table 4.2:

TABLE 4.2 GDL, MPL Physics Properties			
Physics Properties		Unit	Value
Total Cathode gas Diffuser Thickness		μm	300
MPL Porosity	ϵ_{MPL}		0.7
MPL Permeability	K_{MPL}	m^2	1.00e-14
Surface tension liquid-water-air (80°C)	σ	(N/m)	0.0625
cell temperature	T_{cell}	°C	80
Net water transport coef.	α		0.5

4.5 Multilayer Diffusion Media Results

For Multilayer diffusion media a total distance of 300 μm has been considered. Fig 4.5 shows the water saturation considering the total diffusion media where the Micro Porous Layer (MPL) has a thickness of 30 μm which account for the 10% of total thickness; therefore the GDL would be of 270 μm corresponding to the remaining 90% of the total thickness.

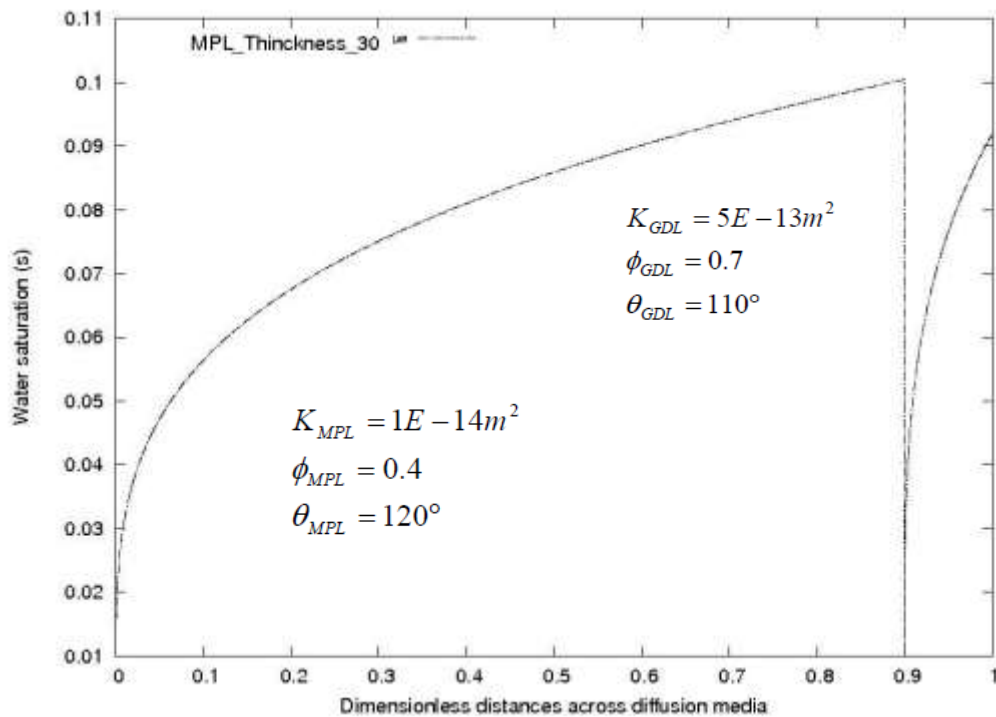


Figure 4.5 Water Saturation Profile along Multilayer GDM

Figure 4.5 depicts how the water saturation decreases at the catalyst layer with the inclusion of a MPL. The lower saturation is clearly understandable due to the change in the material

properties. The water saturation diminution is favorable because it is directly related to the active area where the reduction reaction takes place.

4.5.1 Multilayer analysis Changing Morphological parameters

It is know that changing some morphological parameters we can increase the liquid water transport. It was analyzed the influence of certain parameters as MPL thickness, wettability and porosity in the water transport.

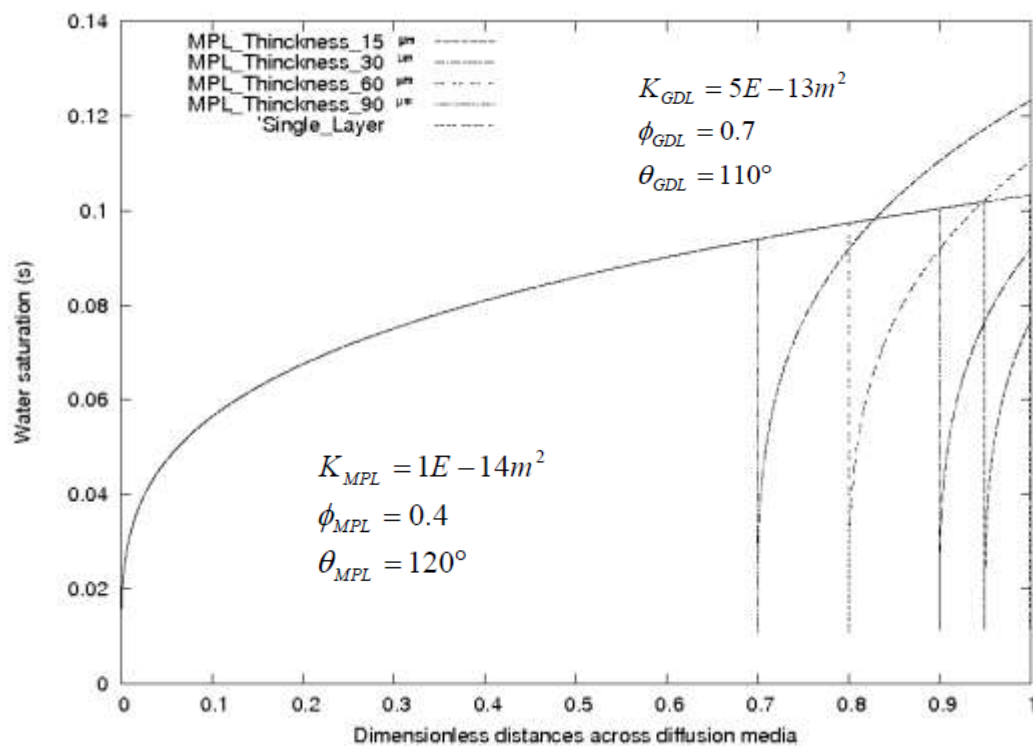


Figure 4.6 Water Saturation Profile along DM Changing MPL Thickness

Figure 4.6 shows the saturation profile of across the Diffusion media at different Micro porous layer thickness. This figure shows that as the MPL thickness increases, the water

saturation increases. We can notice that inserting a MPL of a dimensionless distance of 0.7 and 0.8 of the total thickness the positive effects cancels.

Figure 4.7 shows the water saturation average versus the MPL thickness. In this figure it can be seen that the water saturation is lower between 40 μm and 50 μm .

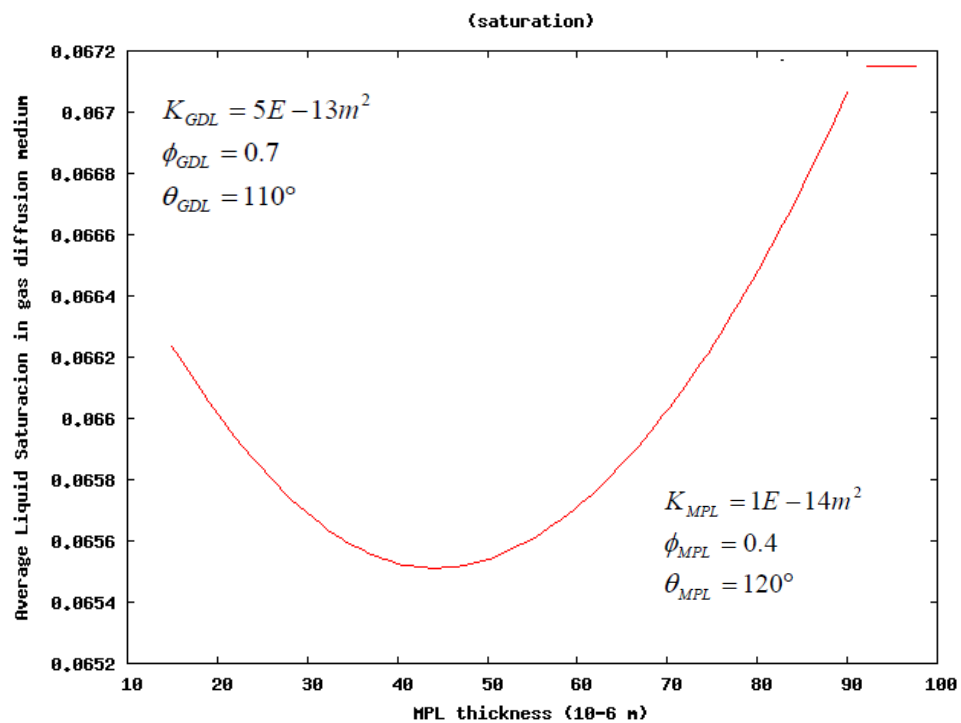


Figure 4.7 Water Saturation Average at different MPL Thickness

The effect of different MPL thickness in the Catalyst Layer-MPL interface is shown in FIG 4.8. It shows by increasing the thickness of MPL, the saturation of the catalyst layer is reduced.

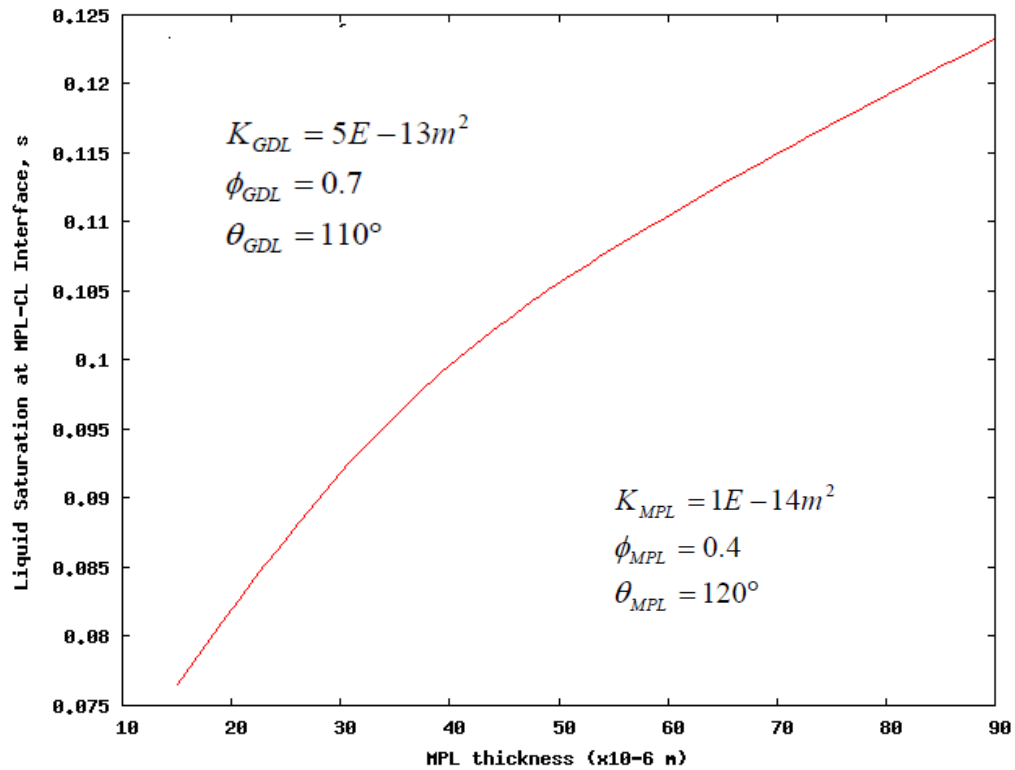


Figure 4.8 Water Saturation at the GDL-CL interface at different MPL Thickness

Another important factor in two-phase transport across the Diffusion media is the porosity. This effect is analyzed in Figure 4.9 by using micro porous layers with different porosities. From figure 4.9 can be noticed that at high MPL porosity, the resistance to liquid water flow in the MPL is smaller, therefore less capillary pressure is needed to drainage the water. Consequently the increase in the liquid saturation in MPL is smaller in larger porosities.

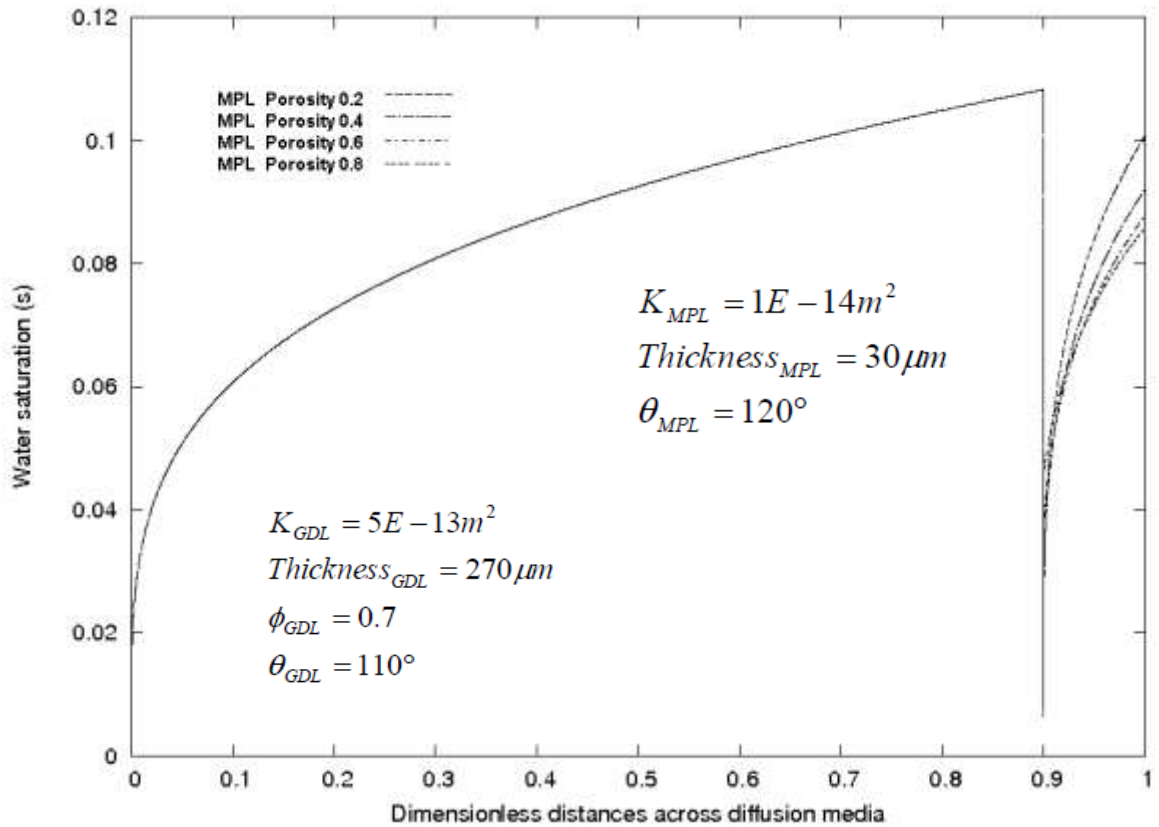


Figure 4.9 Water Saturation along DM at different MPL Porosities

As it was mentioned in the previous chapter the wettability property of the diffusion media is an essential and important parameter in the water transport. The wettability depends on the contact angle between the non-wetting phase (water) and the solid phase (solid). The angle increases as the diffusion media has a higher hydrophobic property.

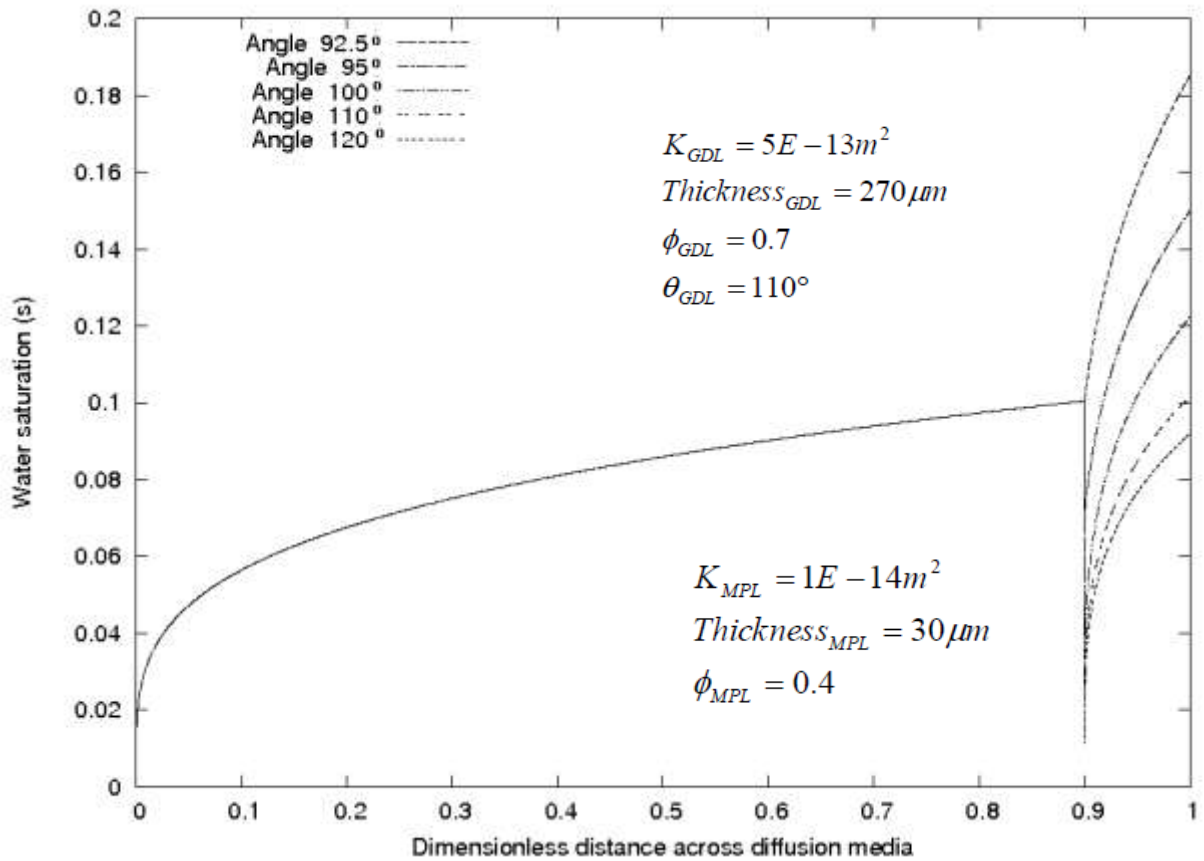


Figure 4.10 Water Saturation along DM at different MPL Contact Angle

Figure 4.10 shows that with a contact angle between 95° and 100° , the discontinuity at the interface between GDL-MPL is reversed and instead of decrease the saturation at the GDL-CL interface a higher saturation is obtained. This effect gets canceled with contact angles above 100° where the discontinuity is enlarged and the water saturation at the catalyst layer-GDL interface decreases.

5 TWO DIMENSIONAL WATER TRANSPORT ANALYSIS FOR SINGLE LAYER DIFFUSION MEDIA

In the present chapter two dimensional analysis of the water transport is discussed. The “land part”, which is the division between channels in a cell stacks, is considered, this land part tends to increase the liquid water saturation due to its no flux condition. Numerical simulations, based on an explicit iterative method, with the same assumption made in the previous chapter, have been performed.

5.1 Methodology

The governing equation for liquid-water transport is based on the continuity equation for steady state condition.

$$\nabla(\rho_l u) = 0 \quad 5.1$$

As in the previous chapter the liquid water flux is expressed by the Darcy`s law. The liquid water pressure is expressed in terms of water saturation using the Unsaturated Flow Theory (UFT) assumption. The liquid pressure is expressed in terms of capillary pressure. The capillary pressure is modeled in terms of water saturation with the Leverett function:

$$u_l = \frac{Kk_{rl}}{\mu_l} \sigma \cos \theta_c \left(\frac{\phi}{K} \right)^{1/2} J(s) \quad 5.2$$

Substituting equation 5.2 into equation 5.1

$$\nabla \cdot \left[\frac{Kk_{rl}}{\nu_l} \sigma \cos \theta_c \left(\frac{\phi}{K} \right)^{1/2} \frac{dJ(s)}{ds} \right] = 0$$

$$\frac{\sigma \cos \theta_c}{\nu_l} (\phi K)^{1/2} \nabla \cdot \left[k_{rl} \frac{dJ(s)}{ds} \nabla s \right] = 0 \quad 5.3$$

Defining C(s) as:

$$c(s) = \left[k_{rl} \frac{dJ(s)}{ds} \right] \quad 5.4$$

Then equation 5.3 is redefined as:

$$\frac{\sigma \cos \theta_c}{\nu_l} (\phi K)^{1/2} \left[\frac{\partial}{\partial x} \left[c(s) \frac{\partial s}{\partial x} \right] + \frac{\partial}{\partial y} \left[c(s) \frac{\partial s}{\partial y} \right] \right] = 0 \quad 5.5$$

Where Equation 5.5 represents the water content in a Gas Diffusion Layer for two dimensions, macroscopic, steady state based on a Darcy's approach model with a Leverett function UFT assumption.

This equation is solved numerically and the corresponding computational domain with its boundary condition will be discussed in the next section.

5.2 Computational Domain and Boundary Conditions

The computational domain used for this analysis is described in figure 5.1. The right part of the computational domain corresponds to the catalyst layer which was assumed to be infinitely thin in comparison to the diffusion media thickness.

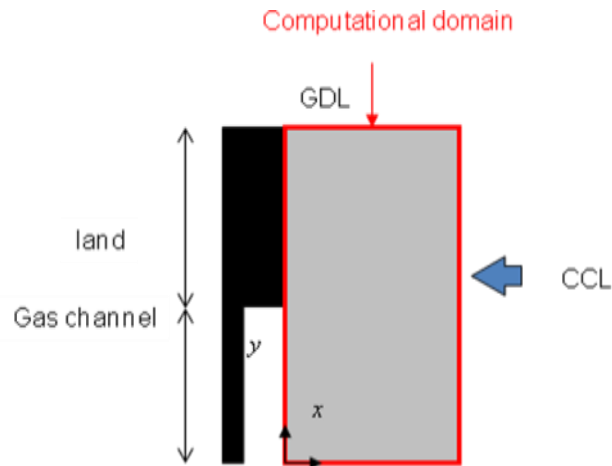


Figure 5.1 Schematic for 2 dimension computational domain, where GDL refers to the gas diffusion layer and CCL refers to cathode catalyst layer

The equation that governs this boundary is:

$$\frac{\sigma \cos \theta_c}{\nu_l} (\phi K)^{1/2} \left[\frac{\partial}{\partial x} \left[c(s) \frac{\partial s}{\partial x} \right] + \frac{\partial}{\partial y} \left[c(s) \frac{\partial s}{\partial y} \right] \right] = -\frac{I}{2F} (2\alpha + 1) M^{H_2O} \quad 5.6$$

Where the α refers to the net water transport from the anode to the cathode, I represent the electric current density which would be a value of 2 A/cm^2 and F and M^{H_2O} represent faraday constant and the molar mass of water respectively. The left part of equation 5.6 corresponds to equation 5.5 which refers to the liquid water flux for interior points and the right part of

the equation 5.6 corresponds to the liquid water inlet due to the oxygen reduction reaction and the net water transport.

The top and the bottom parts are assumed to be symmetric. The symmetry boundary condition is expressed as:

$$\frac{\partial P_c}{\partial y} = 0. \quad 5.7$$

Therefore for the top and bottom boundary the governing equation is reduced to equation 5.8

$$\frac{\sigma \cos \theta_c}{\nu_l} (\phi K)^{1/2} (s^3) \frac{dJ(s)}{ds} \left[\frac{\partial s}{\partial x} \right] = 0. \quad 5.8$$

On the left side of the computational box we have the gas channel and the land. The boundary condition for the gas channel is that the saturation at the Gas Channel-GDL interface is zero ($s=0$). For the land-GDL, the boundary condition is that we have zero flux and it is expressed as:

$$\frac{\partial P_c}{\partial x} = 0. \quad 5.9$$

Therefore for this boundary the equation 5.5 is reduced to:

$$\frac{\sigma \cos \theta_c}{\nu_l} (\phi K)^{1/2} (s^3) \frac{dJ(s)}{ds} \left[\frac{\partial s}{\partial y} \right] = 0 \quad 5.10$$

The boundary conditions are summarized in Figure 5.2.

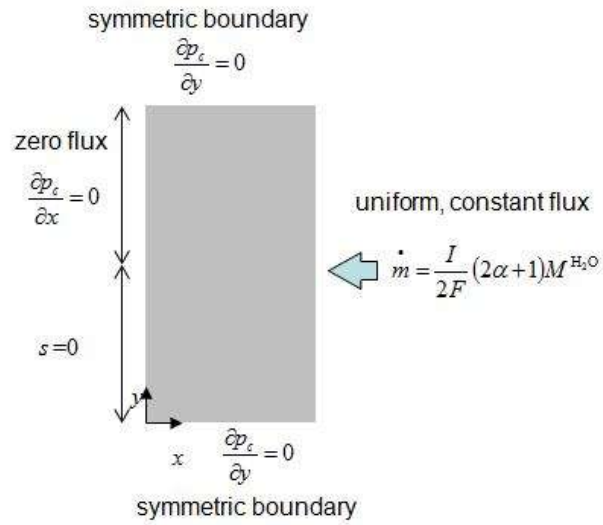


Figure 5.2 Boundary conditions for two dimensional model

The physical properties of the GDL are taken from table4.1:

TABLE 4.3 GDL Physics Properties

Physics Properties		Unit	Value
Total Cathode gas Diffuser Thickness		μm	300
GDL Contact Angle	θ	°	108
GDL Porosity	ϵ_{GDL}		0.4
GDL Permeability	K_{GDL}	m^2	5.00e-13
Surface tension liquid-water-air (80°C)	σ	(N/m)	0.0625
Liquid water viscosity (80°C)	μ_1	(Pa.s)	30
Liquid water desnsity (80°C)	ρ	(Kg/m3)	5
cell temperature	T_{cell}	°C	11
Net water transport coefficient	α		0.5

5.3 Discretization

The governing equation for the internal points is the following:

$$\left[\frac{\partial}{\partial x} \left[c(s) \frac{\partial s}{\partial x} \right] + \frac{\partial}{\partial y} \left[c(s) \frac{\partial s}{\partial y} \right] \right] = 0 \quad 5.11$$

Equation 5.11 has been discretized in a Cartesian orthogonal coordinate system using the staggered second-order finite-difference approximation.

$$\left[C_{(i+0.5,j)} \frac{S_{(i+1,j)} - S_{(i,j)}}{\Delta x} - C_{(i-0.5,j)} \frac{S_{(i,j)} - S_{(i-1,j)}}{\Delta x} \right] \frac{1}{\Delta x} + \left[C_{(i,j+0.5)} \frac{S_{(i,j+1)} - S_{(i,j)}}{\Delta y} - C_{(i,j-0.5)} \frac{S_{(i,j)} - S_{(i,j-1)}}{\Delta y} \right] \frac{1}{\Delta y} = 0 \quad 5.12$$

Rearranging the terms; we obtain:

$$S_{(i,j)} = \frac{C_{(i+0.5,j)} S_{(i+1,j)} + C_{(i-0.5,j)} S_{(i-1,j)} + \left[\frac{\Delta x}{\Delta y} \right]^2 C_{(i,j+0.5)} S_{(i,j+1)} + \left[\frac{\Delta x}{\Delta y} \right]^2 C_{(i,j-0.5)} S_{(i,j-1)}}{C_{(i+0.5,j)} + C_{(i-0.5,j)} + \left[\frac{\Delta x}{\Delta y} \right]^2 C_{(i,j+0.5)} + \left[\frac{\Delta x}{\Delta y} \right]^2 C_{(i,j-0.5)}} \quad 5.13$$

Equation 5.13 was solved using an iterative explicit numerical method [26]. Succeed of the method depends on the accuracy of the initial guess due to the complexity of the equation. The initial guess was taken from the one dimensional analysis.

The computational domain is a uniform grid with a resolution of [200x100]. It can be appreciated that the grid resolution is higher in the X direction than Y direction due to the higher saturation gradient along the X direction in comparison to the saturation gradient in Y direction.

5.4 Results

The results obtained from the numerical solution of the above equation are plotted in Figure

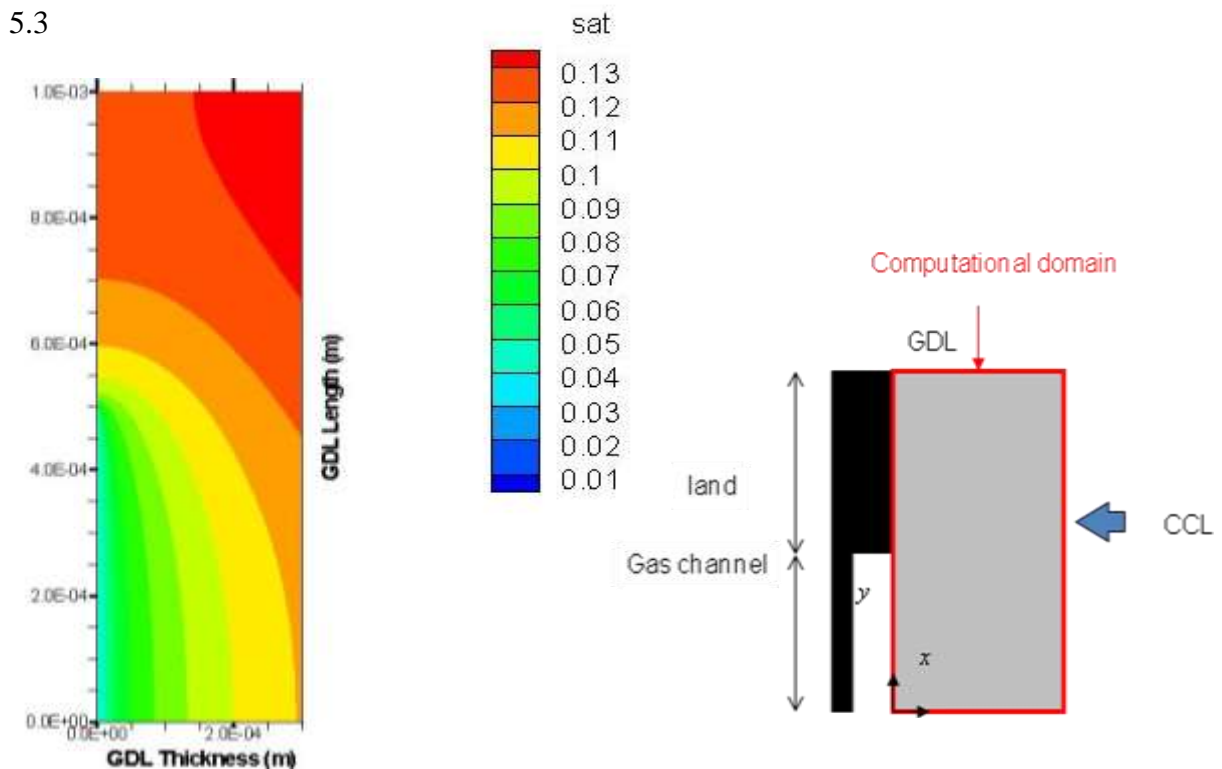


Figure 5.3 two-dimensional water content color contour in a GDL at a current density of 2 A/cm² under standard conditions

The right side of figure 5.3 shows a sketch of the computational domain which helps to understand the results obtained. On the left side of Figure 5.3 color contours of water saturation in a GDL are shown. The left side of the graphics is the GDL-catalyst layer interface. The bottom left part of the contour shows the gas channel-GDL interface where the saturation is zero ($s=0$), the top left part of it represents the land effect. It can be seen an increase of the water saturation with the inclusion of the land effect. This is due to the no flux condition which increases the water saturation at the top part of the GDL. The higher saturation is found at the top right part of the domain where the saturation reaches a value of 0.13.

In order to validate the results the saturation on the bottom boundary of this two dimensional analysis was compared with the one obtained in the one dimensional analysis. The results agree well.

6 EVAPORATION THICKNESS

At high electric current density, the water vapor pressure reaches the saturation pressure, it precipitates becoming liquid. The inverse process occurs near the gas channel where the liquid water under a certain temperature reach a smaller pressure than the evaporation pressure and the liquid water becomes water vapor. The distance from where liquid water starts to appear to the gas channel-GDL interface is called “Evaporation Front” or “Liquid Front”

In the present chapter we obtained analytically the liquid front for one dimension assuming constant temperature for the entire GDL. The effect of different temperatures and different air relative humidity over the liquid front are analyzed. This one dimensional analytical analysis is used as an insight to later implement the evaporation thickness for the two dimensional model.

6.1 Assumptions

- Steady State
- Isothermal
- Two Phase Flow is modeled with unsaturated Flow theory (UTF)
 - Gas Phase pressure is constant across the porous media
- Liquid Phase flux is expressed by Darcy`s Law
- No condensation or Evaporation in gas diffusion media
 - No source/sink terms

- No net gas Phase diffusion
- There exists only one mode at the time to transport water either Liquid or vapor water.
- Where liquid water exists, the water vapor is constant and fully saturated.

The more important assumption for this implementation is that the gas-phase pressure is constant across the porous media.

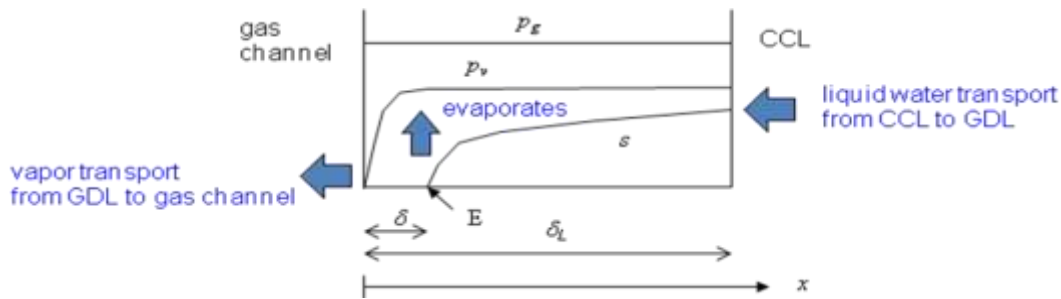


Figure 6.1 Scheme for 1-dimensional evaporation implementation

6.2 Methodology

The governing equation of water vapor flux is expressed by Fick's law:

$$J_v = -\rho D_{vap}^{eff} \nabla m_{vap} \quad 6.1$$

It states that the principal mechanism to transport water vapor is the concentration gradient (∇C_{vap}) thus the relative humidity in the gas channel is a fundamental factor affecting the diffusion of water vapor. The effective diffusivity coefficient (D_{vap}^{eff}) depends of the porosity of the porous media and the diffusivity of the channel:

$$D_{eff} = D \frac{\phi}{\tau} \quad 6.2$$

Equation 6.2 expresses the effective diffusivity in terms of porosity and tortuosity, where ϕ expresses the porosity, D is the binary diffusivity of the gas, and τ is the tortuosity. Tortuosity is a difficult parameter to estimate except through direct experimentation. We assume τ to be proportional to $\phi^{-0.5}$ [8], introducing this expression to the Equation 6.2 it yields.

$$D_{eff} = D\phi^{1.5} \quad 6.3$$

The binary diffusivity coefficient is calculated from Bruggeman correlation which express the diffusivity coefficient in terms of temperature and pressure expressed as:

$$D_{12}(T, P) = D_{12, Known}(T_{ref}, P_{ref}) \left(\frac{T}{T_{ref}} \right)^{3/2} \left(\frac{P_{ref}}{P} \right) \quad 6.4$$

Where the diffusivity is taken from an experimental data and depends on the two gasses acting on it as the temperature and pressure. To perform this analysis a temperature and pressure of 353 K and 1atm respectively were used. For a gas pair of air-water the diffusivity coefficient corresponding to 353K and 1 atm was taken from Y. Wang, C. Y. Wang [22] and it has a value of $2,75e-5 \text{ m}^2/\text{s}$.

We assume that only one transport mechanism exist and this can be as liquid water or water vapor, therefore water vapor remains saturated while liquid water exist. These two assumptions are fundamental in order to find evaporation front that will be located at the place where the liquid flux reach the same value as the water flux.

$$\dot{m}_v = \dot{m}_{ccl} \quad 6.5$$

To perform this one dimensional model, equation 6.1 and left side of equation 4.2 are expressed as follow:

$$\dot{m}_v = \frac{D_{vap}^{eff} (\rho_{sat} - \rho_{GC})}{\delta} \dot{m}_{ccl} \quad 6.6$$

Where the diffusive flux equation is used in terms of mass fraction, \dot{m}_v corresponds to the vapor flux, \dot{m}_{CCL} corresponds to the liquid water flux, ρ_{sat} and ρ_{GC} correspond to the water vapor mass concentration fully saturated and at the gas channel respectively and δ corresponds to the evaporation thickness or liquid front. The evaporation thickness for a single diffusion media (GDL) will be calculated at several temperatures and relative humidity.

6.3 Results

Table 6.1 shows the obtained results from the one dimensional calculation of Evaporation thickness. Temperatures of 20, 40, 50, 60, 80 and 90 °C Celsius and relative humidity of 20, 40, 60, 80 % at the gas channel-GDL interface were considered.

TABLE 6.1 Evaporation Liquid front and diffusivity coefficient

Temperature °C	HR		(%)		D_{vap}^{eff} m^2 / s
	20	40	60	80	
	$\times 10^{-4}$	$\times 10^{-4}$	$\times 10^{-4}$	$\times 10^{-4}$	
20	0.727	0.545	0.363	0.1819	1.97E-05
40	2.37	1.78	1.187	0.593	2.17E-05
50	4.029	3.022	2.014	1.007	2.27E-05
60	6.61	4.96	3.308	1.65	2.38E-05
80	16.18	12.14	8.09	4.046	2.60E-05
90	24.2	18.22	12.14	6.074	2.71E-05

Fixing a diffusion media thickness of $300E-6$ m, liquid water appears at a temperatures lowers than $60^{\circ}C$ for certain RH conditions and for temperatures lower than $40^{\circ}C$ for all the HR showed in table 6.1.

Figure 6.2 depicts the different evaporation thickness for different gas channel relative humidity at different temperatures. It can be seen that with the increase of the temperature the evaporation thickness increases therefore less liquid water is found in the GDL. The opposite effect is caused by the relative humidity. The higher is the relative humidity the smaller is evaporation thickness.

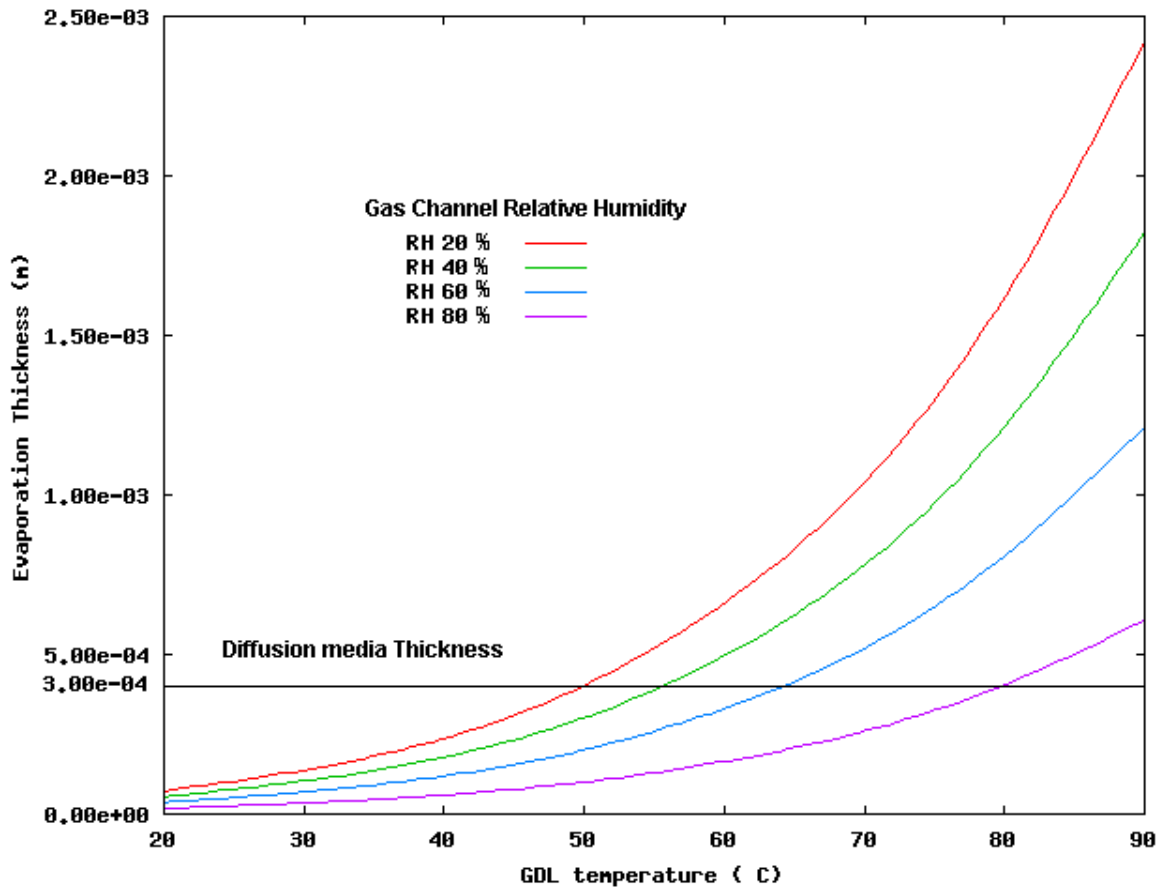


Figure 6.2 Evaporation thickness vs. temperature for different RH

The evaporation thickness for a temperature of 40°C and a relative humidity of 60 % at the gas channel it is show in FIG 6.3. From Table 6.1 we asses that the evaporation thickness is 1.187E-4m and we can appreciate how the vapor concentration is fully saturated until the liquid water reaches the evaporation pressure.

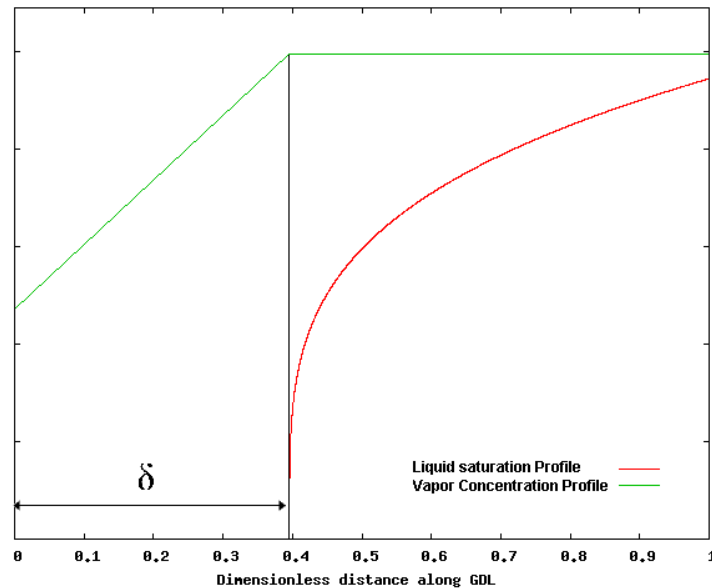


Figure 6.3 Scheme of Liquid saturation and vapor concentration flux

6.4 Two dimensional Liquid front

The challenge in implementing the evaporation front for the two dimensional model is to match the vapor and liquid fluxes in the two orthogonal directions. The procedure in order to obtain the evaporation thickness is:

- Guess the Evaporation thickness.
- Calculate the water saturation and vapor concentration based in the guess evaporation front
- Calculate the flux of each of the two phases and compare these two fluxes
- If it does not match move the evaporation thickness and repeat until those match

The water saturation was solved using the approach already described in chapter 3 and 4 and the vapor mass concentration was modeled using Fick's law.

6.5 Two dimensional Liquid front Methodology

The vapor phase is modeled using Fick's law. For 2 dimensions:

$$\nabla \cdot [D_{vap}^{eff} \nabla m_{vap}] = 0 \quad 6.7$$

Where the amount or concentration of vapor is quantified in terms of its mass density ρ (Kg/m^3).

$$\nabla \cdot \left[\frac{D_{vap}^{eff}}{M} \nabla \rho_{vap} \right] = 0 \quad 6.8$$

Assuming constant temperature in all the domain and rearranging equation 6.8; we obtain:

$$D_{vap}^{eff} \left[\frac{\partial \rho_{vap}^2}{\partial x^2} + \frac{\partial \rho_{vap}^2}{\partial y^2} \right] = 0 \quad 6.9$$

Equation 6.9 represents the two dimensional vapor diffusion in a single layer diffusion media (GDL). The boundary conditions for this equation will be shown in the next section

6.6 Boundary Conditions for two dimensional model

The boundary conditions for the 2d model follow the assumptions made at the beginning of the chapter. The right boundary just after the evaporation front is assumed to be fully saturated ($\rho_{vap} = \rho_{sat}$). The left boundary of the computational box has two boundary conditions. From the half of the domain to the top, zero flux is assumed and it is expressed as:

$$\frac{\partial \rho_{vap}}{\partial x} = 0 \quad 6.10$$

From the half of the domain to the bottom, $s=0$ is imposed. On the lower and upper boundary of the computational box, a condition of symmetry is assumed:

$$\frac{\partial \rho_{vap}}{\partial y} = 0 \quad 6.11$$

The all boundary conditions for this two dimensional analysis are shown in Fig 6.4 to help the reader:

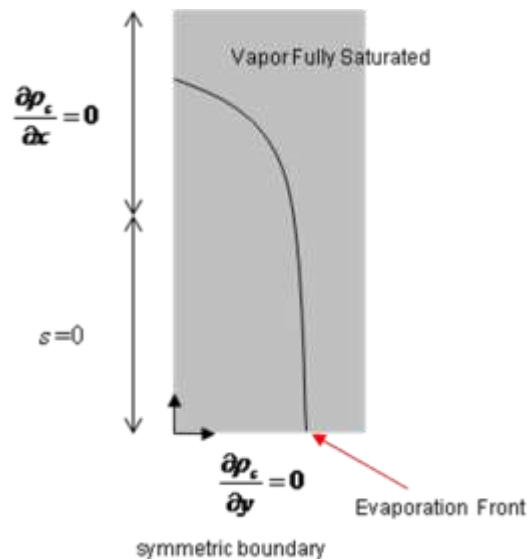


Figure 6.4 Scheme of 2-dimensional domain boundary conditions

6.7 Two dimensional diffusion equation discretization

The vapor diffusion equation in an orthogonal coordinate system for the central interior point is:

$$D_{vap}^{eff} \left[\frac{\partial \rho_{vap}^2}{\partial x^2} + \frac{\partial \rho_{vap}^2}{\partial y^2} \right] = 0 \quad 6.12$$

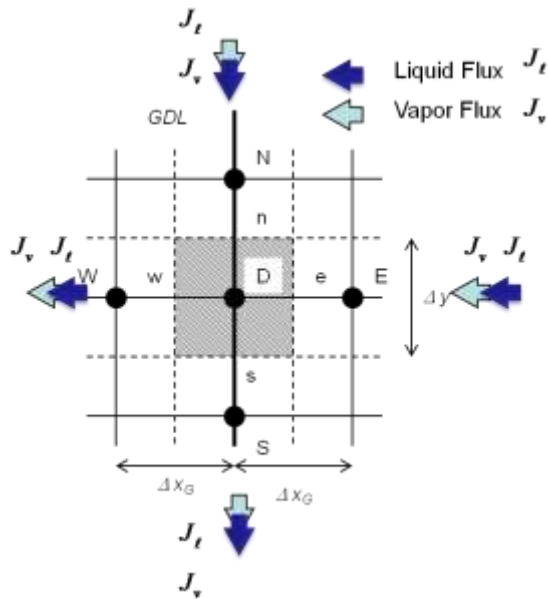
Discretizing the equation, Using central finite difference and uniform mesh we obtain:

$$\frac{D \cdot [\rho_{(i+1,j)} + \rho_{(i-1,j)} - 2\rho_{(i,j)}]}{\Delta x^2} + \frac{D \cdot [\rho_{(i,j+1)} + \rho_{(i,j-1)} - 2\rho_{(i,j)}]}{\Delta y^2} = 0 \quad 6.13$$

Rearranging for the central point:

$$\rho_{(i,j)} = \frac{\rho_{(i+1,j)} + \rho_{(i-1,j)} + \rho_{(i,j+1)} \left[\frac{\Delta x^2}{\Delta y^2} \right] + \rho_{(i,j-1)} \left[\frac{\Delta x^2}{\Delta y^2} \right]}{2 \left[1 + \left[\frac{\Delta x^2}{\Delta y^2} \right] \right]} \quad 6.14$$

This expression has been solved using a numerical explicit iterative method [26]. The computational domain, grid sizes are the same. Liquid water and water vapor flux are calculated and matches as the figure 6.5 shows.



$$J_v = -D_{vap}^{eff} \nabla C_{vap}$$

$$J_l = \rho_l u_l = \frac{Kk_{rl}}{v_l} \nabla p_c$$

Figure 6.5 Scheme of two dimensional matching flux

The liquid front will readjust each time until the liquid flux matches with the vapor flux. The boundary conditions from the liquid saturation and vapor concentration will readjust depending on the direction where the evaporation front is moving. The process is repeated for a number of iterations sufficient to reach convergence.

6.8 2-Dimensional Results

Figure 6.6 illustrates the water content into the GDL assuming evaporation. The blue color in the water saturation contour represents no water content in the GDL, and as a result of the not sink and source assumption blue contours represent the vapor present in the GDL.

It was compared the bottom vapor and water saturation profile with the obtained in the 1-dimensional analysis. The agreement validates the present results. In figure 6.6 it can be appreciated that the water content at the catalyst layer increases at the land ratio but decreases close as it gets closer to the gas channel. The water saturation increase is due to the no flux boundary condition which was mentioned in chapter 5 when it was analyzed the water saturation without taking into account evaporation.

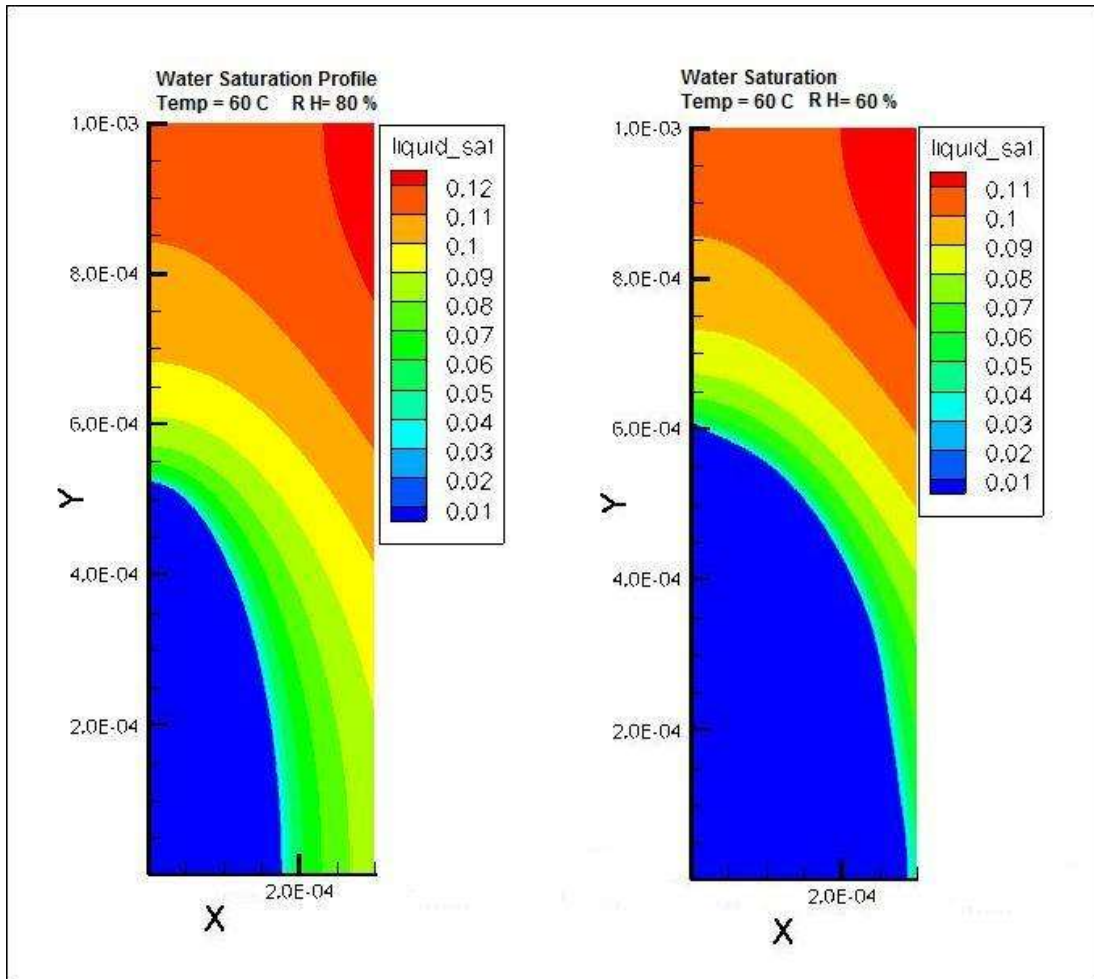


Figure 6.6 2-dimensional contour water saturation implementing evaporation at different RH

Fig 6.6 also illustrates how the evaporation thickness decreases as the relative humidity increases. This is due to the decrease of concentration gradient which directly causes a reduction of water vapor flux.

Figure 6.7 shows vapor concentration in terms of mass density corresponding to the same case as Figure 6.6 where the red contour means that vapor is fully saturated and it begins to decrease right after the liquid water ends at the evaporation front until the value corresponding to the gas channel vapor density.

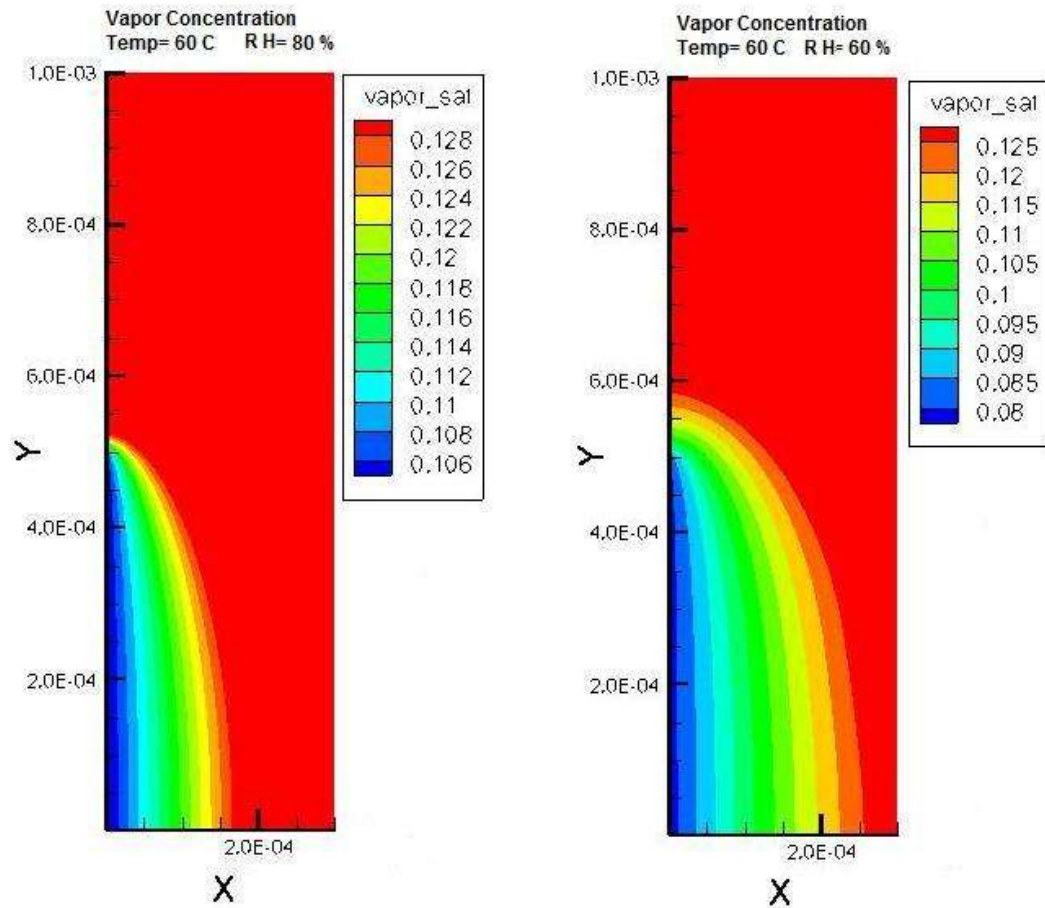


Figure 6.7 2-dimensional contour vapor concentrations in terms of density at different RH

In figure 6.8 the variation of the evaporation thickness for different temperatures at a fix relative humidity of 80% is shown. It can be appreciated that the evaporation thickness increases as the temperature increases due to the fact that temperature directly affects the evaporation pressure and with it the water evaporation thickness.

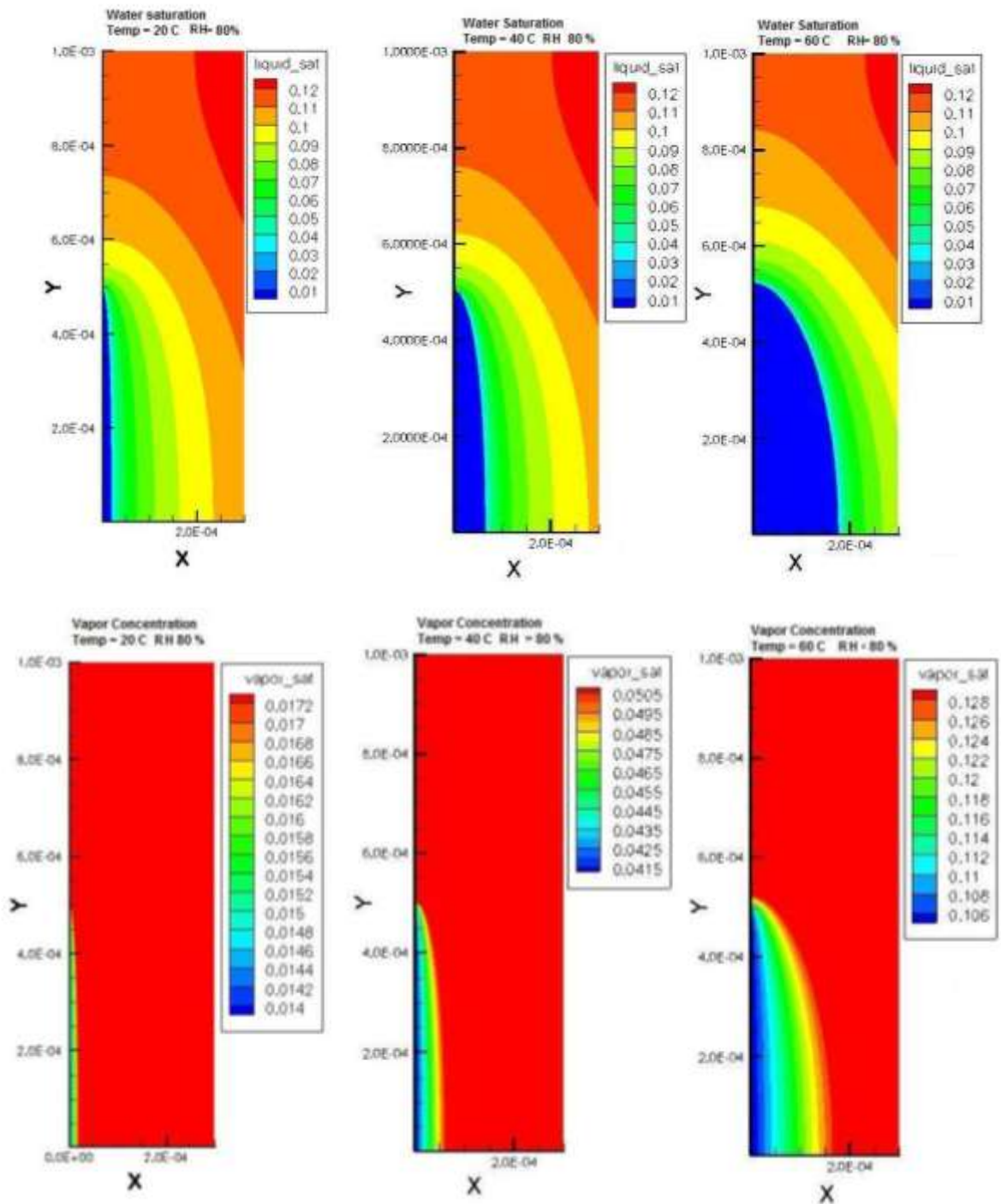


Figure 6.8 2-dimensional water saturation and vapor concentration at different GDL Temperatures.

7 CONCLUSIONS

The modeling of water transport in a porous media is still under research, because of the lack of experimental data that could serve as a reference point in order to validate the numerical predictions. Water flux and water content can be estimated by proposing certain assumptions. The water transport can be modeled it with an experimental correlation which is the usually called Leverett function.

The insertion of a porous media, as the carbon cloth or carbon paper, in to the fuel cell is fundamental to its efficiency, since the porous media provides the necessary drainage to the liquid water. Water is the product of the limited reaction at the cathode side, and its drainage becomes more important near the catalyst layer. The reaction is limited because the production of water is higher than the consumption of hydrogen.

Even though this model is ideal, important conclusions can be made with the results of this study. Beside of been an ideal model, the present study constitutes an excellent starting point for future research and implementation of more features to the model.

From the one dimensional section were obtained the following conclusions:

The morphological properties of the porous material affect the water content and its respective drainage in order to prevent the undesirable flooding. The insertion of Multilayer with different characteristics creates a discontinuity on the physical properties and the performance of water drainage at the threshold which is at the catalyst layer. This is

demonstrated in section 4.4.1 where the effects of thickness, porosity, and wettability as a function of the contact angle were analyzed.

It was found that as MPL thickness increases, the water saturation also increases and that at MPL with thickness less than $30\mu\text{m}$ we can obtain a decrease in the water saturation. At values higher than $30\mu\text{m}$ the positive effect cancels. In relation with the water saturation average in the entire diffusion media, it was found lower values, between 0.7 and 0.8, of the total diffusion media thickness. At the catalyst layer, the thinner it gets the less water saturation is found at the MPL.

The same section also treats the effect of the discontinuity in the porosity. It was found that at higher MPL porosities, the resistance of liquid water to the flow is smaller, therefore less capillary pressure to drainage is required. Finally, it was analyzed the effect of the angle of contact. It was found that at an angle below 90 and 100 degree, the effect of drainage becomes negative.

In the 2 dimensional analyses, it was found that the land effect increases the water content reaching higher water saturation values at the top of the domain where the land is located. This analysis can be found in section 5.5.

With the implementation of the evaporation thickness an additional phase is introduced to the problem. The case can be treated as one phase with the assumption that just one movement mechanism can move the water at the time. In section 6.4 it was found analytically the distance from the gas channel where the liquid water changes phase and becomes vapor by neglecting the transition effect.

Table 6.1 and figure 6.2 shows the different values of evaporation thickness at different temperatures and RH. With the temperature increase, the evaporation thickness increases and as the RH increases the evaporation thickness decreases. Finally at section 6.9 it was analyzed the same effect over a two dimensional model and it was found that at high temperature and low evaporation thickness the liquid saturation level is relatively higher at the land side of the domain. This occurs because of the no flux effect of the land.

REFERENCE

1. J.M. Andujar, F. Segura , Fuel cells: History and updating. A walk along two centuries, Renewable and Sustainable Energy Review Vol 13, pp 2309-2322, 25 march 2009
2. PG. Grimes. Historical Pathways for fuel cells. IEEE Aerospace and Electronic Systems Magazine Vol 15 pp 1-10 December 2000
3. <http://www.fuelcells.org/info/charts/buses.pdf>
4. Corey T. Arthur, Mechanics of Immiscible Fluids in Porous Media, Water Resources Publications, LLC,
5. Jacob Bear, Dynamics Of fluids in porous media, American Elsevier publishing company, Inc
6. Robert A. GreenKorn, Flow Phenomena in Porous Media, Fundamentals and Applications in petroleum, water and food production, Marcel Dekker, Inc, First edition.
7. Incropera Dewitt, Bergman Lavine Fundamentals of Heat and mass transfer, Editorial John Wiley & Sons, sixth edition
8. Matthew M. Mench Fuel Cell Engines, Editorial John Wiley & Sons, First edition
9. F.A.L. Dullien Porous media fluid transport and pore structure, Academic Press, Second edition

10. Jeffrey T. Gostick a, Michael W. Fowler a,* , Marios A. Ioannidis a, Mark D. Pritzker a, Y.M. Volkovich b, A. Sakars b "Capillary pressure and hydrophilic porosity in gas diffusion layers for polymer electrolyte fuel cells" Journal of power sources vol 156 pp 375-387, 15 July 2005
11. E.C. Kumbur, K.V. Sharp, M.M. Mench On the effectiveness of Leverett approach for describing the water transport in fuel cell diffusion media, Journal of power sources Vol 168 pp 356-368, 2 march 2007
12. Wensheng He, Jung S. Yi, and Trung Van Nguyen Two-Phase Flow Model of the Cathode of PEM Fuel Cells Using Interdigitated Flow Fields, Materials, Interfaces, and electrochemical phenomena, Vol 46 pp 2056-2064, October 2000
13. Ugur Pasaogullari* and C. Y. Wang**, Liquid Water Transport in Gas Diffusion Layer of Polymer Electrolyte Fuel Cells, Journal of the Electrochemical Society Vol 151 pp A399-A406, 5 February 2004.
14. F. Y. Zhang, X. G. Yang,* and C. Y. Wang*, Liquid water removal from a Polymer electrolyte fuel cell, Journal of the Electrochemical Society Vol 153, A225-A232 September 6, 2005
15. Z.H. Wang, C.Y. Wang,* , K.S. Chen Two-Phase flow and transport in the air cathode of proton exchange membrane fuel cells, Journal of power sources Vol 94 pp 40-50, September 29, 2000
- 16 Puneet K. Sinha, Chao-Yang Wang Liquid water transport in a mixed-wet gas diffusion layer of a polymer electrolyte fuel cell, Chemical Engineering Science vol 63 pp 1081-1091, November 13, 2007
17. Ugur Pasaogullari, Chao-Yang Wang* Two-phase transport and the role of micro-porous layer in polymer electrolyte fuel cells, Electrochimica Acta Vol 49 pp 4359-4369, 2 june 2004
18. U.S. Department of energy, Office of Fossil and National Energy Technology Energy Fuel Cell Handbook, October 2000

19. S. Lister, G. McLean, PEM fuel cell electrodes , Journal of Power Sources, Vol 130 pp 61-67, 14 December 2003
20. K. Kordesch, G. Simader, Fuel cell and Their applications, Wiley-VCH; 1 edition (March 25, 1996)
21. C. Y. Wang , Fuandemantal for fuel cell engineering, Chem Rev (2004) 104, 4727-4766
22. Y. Wang, C. Y. Wang, Modeling Polymer electrolyte fuel cell with large density and velocity changes, Journal of the electrochemical society 152 (2) (2005) A445-A453
23. Z.Y. Su, C.T. Liu, H.P. Chang, C.H. Li , K.J. Huang, P.C. Sui, A numerical investigation of the effects of compression force on PEM fuel cell performance, Journal of Power Sources 183 (2008) 182-192
24. V. Starikovicius, The multiphase flow and heat transfer in porous media, Berichte des Fraunhofer ITWM, Nr 55 (2003)
25. C. J. Geankoplis, Transport Processes, Momentum, Heat and mass, Editorial Allyn and Bacon.
26. J. D. Hoffman, Numerical Methods for Engineers and Scientist, Editorial Marcel Dekker, Second Edition

APPENDIX A. WATER SATURATION CODE

```
do while (abs(residual_remain).gt.tol)

!!!!!!!!!!!!!!!!!!!!!!!!!!!!!!!!!!!!!!!!!!!!!!!!!!!!!!!!!!!!!!!!!!!!1
C liquid front boundary condition
!makes 0 all the points before the liquid front

      do j=1,my
        th1=th(j)
        do i=1,th1
          ss(i,j)=0.0
        enddo
      enddo

!!!!!!!!!!!!!!!!!!!!!!!!!!!!!!!!!!!!!!!!!!!!!!!!!!!!!!!!!!!!!!!!!!!!
!BBoundary for the left corner of the boundary!

      do j=1,my
        if(th(j).eq.1)then
          if(j.gt.(my/2))then
            ss(1,j)=ss(2,j)
          endif
        endif
      enddo

!!!!!!!!!!!!!!!!!!!!!!!!!!!!!!!!!!!!!!!!!!!!!!!!!!!!!!!!!!!!!!!!!!!!
* Boundary condition for y=0  dp/dy=0
!bottom boundary

      j=2
      do i=(th(1)+1),mx
        ss(i,j-1)=ss(i,j)
      enddo

!top boundary

      j=my
      do i=(th(my)+1),mx
        ss(i,j)=ss(i,j-1)
      enddo
```

```

!reach the water saruration in all the interior points.
  do j=2,my-1
    th1=th(j)
    do i=th1+1,mx-1
c-----east
      ss1=0.5*(ss(i,j)+ss(i+1,j))
      djds=1.417-2.12*2.0*ss1+1.263*3.0*ss1*ss1
      rel_perm=ss1**3.0
      csig=coef_0*rel_perm*djds
c-----west
      ss1=0.5*(ss(i-1,j)+ss(i,j))
      djds=1.417-2.12*2.0*ss1+1.263*3.0*ss1*ss1
      rel_perm=ss1**3.0
      cant=coef_0*rel_perm*djds
c-----north
      ss1=0.5*(ss(i,j)+ss(i,j+1))
      djds=1.417-2.12*2.0*ss1+1.263*3.0*ss1*ss1
      rel_perm=ss1**3.0
      csigy=coef_0*rel_perm*djds
c-----south
      ss1=0.5*(ss(i,j-1)+ss(i,j))
      djds=1.417-2.12*2.0*ss1+1.263*3.0*ss1*ss1
      rel_perm=ss1**3.0
      canty=coef_0*rel_perm*djds
c
      ss(i,j) = csig*ss(i+1,j)+cant*ss(i-1,j)
      $      +csigy*rdxdy2g*ss(i,j+1)+canty*rdxdy2g*ss(i,j-1)
      ss(i,j) = ss(i,j)/(csig+cant+rdxdy2g*csigy+rdxdy2g*canty)

!!!!!!!!!!!!!!!!!!!!!!!!!!!!!!!!!!!!!!!!!!!!!!!!!!!!!!!!!!!!!!!!!!!!!!!!!!!!

      enddo
    enddo

! Reach the water saturation at the right boundary (generation boundary)
!!!!!!!!!!!!!!!!!!!!!!!!!!!!!!!!!!!!!!!!!!!!!!!!!!!!!!!!!!!!!!!!!!!!!!!!!!!!
      i=mx
      do j=1,my

      ss1=0.5*(ss(i-1,j)+ss(i,j))
      djds=1.417-2.12*2.0*ss1+1.263*3.0*ss1*ss1
      rel_perm=ss1**3.0
      cant=coef_0*rel_perm*djds
c-----north
      ss1=0.5*(ss(i,j)+ss(i,j+1))
      djds=1.417-2.12*2.0*ss1+1.263*3.0*ss1*ss1
      rel_perm=ss1**3.0
      csigy=coef_0*rel_perm*djds

```

```

c-----south
    ss1=0.5*(ss(i,j-1)+ss(i,j))
    djds=1.417-2.12*2.0*ss1+1.263*3.0*ss1*ss1
    rel_perm=ss1**3.0
    canty=coef_0*rel_perm*djds
c
    ss(i,j) = cant*(dy/dx)*ss(i-1,j)+csigy*0.5*(dx/dy)*ss(i,j+1)
$           +canty*0.5*(dx/dy)*ss(i,j-1)-prod*dy
    ss(i,j) = ss(i,j)
$           /(cant*(dy/dx)+csigy*0.5*(dx/dy)+canty*0.5*(dx/dy))
    enddo

! reach for the major residual
! num is the iteration number
! s(i,j) is where I save the iteration num-1
    do j=1,my
        do i=1,mx
            residual = abs(ss(i,j)-s(i,j))
                residual=residual/s(i,j)
            if (residual.gt.residual_remain)then
                residual_remain=residual
                posx=i           ! save which point has the bigger residual
                posy=j           !
            endif
            s(i,j)=ss(i,j)
        enddo
    enddo

enddo

```